Magnetospheric location of the equatorward prebreakup arc

V. Sergeev,[1] Y. Nishimura,[2,3] M. Kubyshkina,[1] V. Angelopoulos,[4] R. Nakamura,[5] and H. Singer[6]

Received 10 September 2011; revised 9 November 2011; accepted 11 November 2011; published 25 January 2012.

[1] We address the long-standing problem of the location and origin of the equatorwardmost Pre-Breakup auroral Arc (PBA) by combining energetic particle observations from NOAA Polar Operational Environmental Satellites (POES) overpasses of prebreakup arcs with auroral imaging and magnetospheric observations from the Time History of Events and Macroscale Interactions during Substorms (THEMIS) mission. The prebreakup arc was observed within a few minutes of auroral breakup and ~1–2 hours in MLT from the breakup meridian. For three ideal conjunctions out of 16 PBA crossings, we also construct a dynamically-adapted magnetospheric model after adding concurrent magnetic observations by the GOES spacecraft. Model-predicted isotropy boundaries of energetic particles are compared with observations, informing us about model uncertainties. Direct mapping with adapted models as well as particle flux comparisons between the ionosphere and the magnetosphere confirm that the PBA source lies within the region of the steep equatorial magnetic field gradient, where the equatorial field is also small (5–20 nT). That equatorial location, at roughly 8–10 Re, is likely the earthwardmost edge of the thin cross-tail current sheet. From observations we find that the prebreakup arc nearly coincides in latitude with the energy-dispersed, 30–300 keV electron isotropy boundary. Here the non-adiabatic electron precipitation from the high flux region of the outer radiation belt near its outer edge produces a narrow, intense energetic electron precipitation region, called the energetic electron arc (EEA). Two fortuitous conjunctions with DMSP also confirm that energetic (>20 keV) EEA electrons and lower energy, inverted-V electrons associated with the PBA are collocated. We suggest that EEA formation is an inherent part of the PBA formation process. By creating an enhanced conductance strip, the EEA (a seed arc) produces ionospheric polarization that leads to field-aligned current generation and associated field-aligned electron precipitation. We also discuss implications of our findings for the substorm onset mechanism.

Citation: Sergeev, V., Y. Nishimura, M. Kubyshkina, V. Angelopoulos, R. Nakamura, and H. Singer (2012), Magnetospheric location of the equatorward prebreakup arc, *J. Geophys. Res.*, *117*, A01212, doi:10.1029/2011JA017154.

1. Introduction

[2] The equatorial location and formation mechanism of the equatorwardmost auroral arc, which brightens and breaks up first during substorms [*Akasofu*, 1964], are long-standing unanswered questions in magnetospheric physics. At least three observational difficulties make these questions especially challenging. First, the instability responsible for the rapid auroral brightening occurs in a localized region within the vast expanse of the equatorial magnetotail. For purposes of this paper, the onset of this instability will be assumed to be co-incidental with substorm breakup, auroral expansion onset, and substorm onset, even though they can be temporally resolved [see, e.g., *Angelopoulos et al.*, 2008]. The location can not be definitively established with only "in situ" observations, because several spacecraft provide a relatively sparse sampling of the tentative onset region. Conversely, auroral global imaging alone cannot provide definitive answers regarding the equatorial drivers because auroral intensifications are indirect consequences of equatorial phenomena. Combining in situ spacecraft observations with contextual auroral observations, however, can establish more accurately the location and timing of the equatorial phenomena relative to auroral brightening.

[3] Second, establishing a time-dependent link between ionospheric and magnetospheric phenomena requires knowledge of the magnetic configuration and dynamics. Mapping

[1]Institute of Physics, St. Petersburg State University, St. Petersburg, Russia.
[2]Department of Atmospheric and Ocean Sciences, University of California, Los Angeles, California, USA.
[3]Solar-Terrestrial Environment Laboratory, Nagoya University, Nagoya, Japan.
[4]Department of Earth and Space Sciences and Institute of Geophysics and Planetary Physics, University of California, Los Angeles, California, USA.
[5]Space Research Institute, Austrian Academy of Sciences, Graz, Austria.
[6]NOAA, Boulder, Colorado, USA.

0148-0227/12/2011JA017154

of the auroral intensification region into the magnetosphere is uncertain, however, because the magnetospheric configuration of the interface between tail-like and dipolar field lines around ~10 Re (the "transition" region) is: (1) strongly modified relative to statistical models during the substorm growth phase, and (2) rapidly changing during the course of the breakup. Empirical magnetospheric models based on statistical averages of data are not suitable for such a task. As breakup approaches, an ion gyroradius scale-size, thin current sheet (TCS) may form near the transition region [*Sergeev et al.*, 1990]. There is also evidence of a local magnetic field minimum near that region [*Saito et al.*, 2010]. Absent in standard magnetospheric models, such features can be reconstructed (to some extent) using dynamically-adaptive magnetospheric modeling, in which model parameters are varied at each time step to obtain the best agreement with observed magnetic fields at multiple locations [*Kubyshkina et al.*, 2011]. Even with such models, the localized, rapidly-changing magnetic field following breakup cannot be reproduced perfectly. Dynamically-adaptive models are more suitable for the slowly-varying growth phase current system, however. Since in this paper we focus our attention on the prebreakup, quiet arc, rather than on post-breakup active auroras, we stand to benefit from dynamically-adaptive magnetospheric modeling techniques.

[4] Third, because such modeling relies on a small number of spacecraft, independent evaluation of a model's accuracy is quite important. Such an evaluation can be done by using low-altitude spacecraft to observe pitch angle isotropy boundaries (IBs) of energetic particles and comparing these observations with model-based predictions of those boundaries in the ionosphere [e.g., *Shevchenko et al.*, 2010].

[5] Since analysis of pitch angle isotropy boundaries of energetic particles is critical to this study, we start by showing Figure 1, which exemplifies the basic facts known about these boundaries from observations. These observations were made by the low-altitude (850 km) NOAA-19 spacecraft as it crossed the auroral zone poleward near midnight just prior to an auroral breakup. (Companion satellite and ground observations are described in section 2). The combined region of visible aurora (approximately indicated by a solid fill) indicates that the width of the auroral oval is ~7° latitude (between 64° and 71° GMLat). In the part of the oval poleward of about 65.5°, the precipitating (0° pitch angle, red lines) and trapped (90° pitch angle, black lines), >30 keV particle fluxes are nearly equal, although they remain at low level, characteristic of their origin in the tail current sheet (CS). The radiation belt (RB) region in the equatorward part of the oval is, however, characterized by a very high flux of trapped particles and only weak precipitation. The boundaries between the two regions (CS and RB), called isotropy boundaries, are rather abrupt and well-defined for particles of all energies. However, for a given species, the IBs are observed at systematically higher latitudes for particles of lower energy. For a given energy, the IB for electrons is at higher latitude than that for ions. This IB latitude dependence on energy and species is consistent with the dependence of equatorial particle pitch angle scattering on particle rigidity G ($G = mV/e$, where V is the particle speed).

[6] The latitude variation of the precipitating energy flux peak of thermal plasma sheet protons (0.05 to 20 keV; Figure 1, green curve), is similar to the precipitation of energetic (>30 keV; red curves) protons: their peak flux latitude increases with decreasing energy. The peak in auroral proton precipitation (called the "b2i" boundary) corresponds to the IB at that energy, as established by *Newell et al.* [1998].

[7] This well-ordered picture is known to originate in the properties of single particle motion in the magnetosphere [see, e.g., *West et al.*, 1978; *Sergeev and Tsyganenko*, 1982; *Sergeev et al.*, 1983a]. The inner magnetosphere's strong magnetic field renders particle motion there adiabatic. Loss cone fluxes (red traces in Figure 1) are thus generally small because particles rarely scatter into the loss cone. Trapped fluxes (black traces, at ~90° pitch angle) are rather large, however, since particles are in relatively stable drift orbits. At large distances (near the magnetotail current sheet), the equatorial magnetic field is weak, and particles experience strong pitch angle scattering even during one crossing of the equator. This results in nearly isotropic distributions, also evidenced by red and black traces which nearly coincide at high latitudes. The boundary between two regimes of particle motion (adiabatic and non-adiabatic) occurs where the ratio of radius of curvature R_c to particle gyroradius ρ (both taken at the neutral sheet) is $R_c/\rho \sim 8$ [*Sergeev et al.*, 1983a; *Delcourt et al.*, 1996]. Expressed in terms of the equatorial magnetic field, this results in $R_c/\rho = B_z^2(G * dB_r/dz)^{-1} \approx 8$, which in the current sheet can be cast in terms of the cross-tail current density j as $R_c/\rho \approx B_z^2(G * \mu_0 * j)^{-1} \approx 8$. Thus, the ratio that determines particle scattering depends on the equatorial B_z (squared) and electric current density j. Correspondingly, particles of smaller rigidity ($\rho = G/B$) will have their isotropy boundaries farther in the tail. For example, on average, the IBs of 80 keV protons remain at 5–8 Re at the nightside and those of 100 keV electrons at around 8–12 Re [e.g., see *Shevchenko et al.*, 2010, Figure 2]. IB location may, however, move considerably depending on the magnetic model, especially for electrons.

[8] Many properties of the equatorward prebreakup arc and the isotropy boundaries are illustrated in Figure 1. First, this arc (the auroral electron peak in the first panel denoted by a solid vertical line) occurs near the equatorward part of the auroral oval [*Akasofu*, 1964], so it should map near the Earth, well within the closed field-line region. Second, the arc also appears close (here within 40 km [see also *Dubyagin et al.*, 2003] to the peak of proton precipitation (b2i in Figure 1) [see also *Samson et al.*, 1992; *Donovan et al.*, 2008]. Although its proximity to the peak of proton precipitation is often interpreted as evidence of its proximity to the ring current, this is not valid because the peaks in the latitudinal distributions of precipitated and trapped proton energy flux can be at very different locations [e.g., *Ganushkina et al.*, 2005]. It has also been noted that the equatorwardmost arc is often bounded on its equatorward side by an arc-like band of energetic electron precipitation, as observed independently by X-ray precipitation, riometer absorption, or D-region ionization in the ionosphere [see, e.g., *Pytte et al.*, 1976; *Sergeev et al.*, 1983b, 1990; *Kirkwood and Eliasson*, 1990; *Jussila et al.*, 2004]. Figure 1 shows that this energetic electron arc (EEA), demarcated by the sharp peak in the precipitating energetic electron flux, actually remains near the electron IB. On the other hand, the electron IB stays near the poleward edge of but within

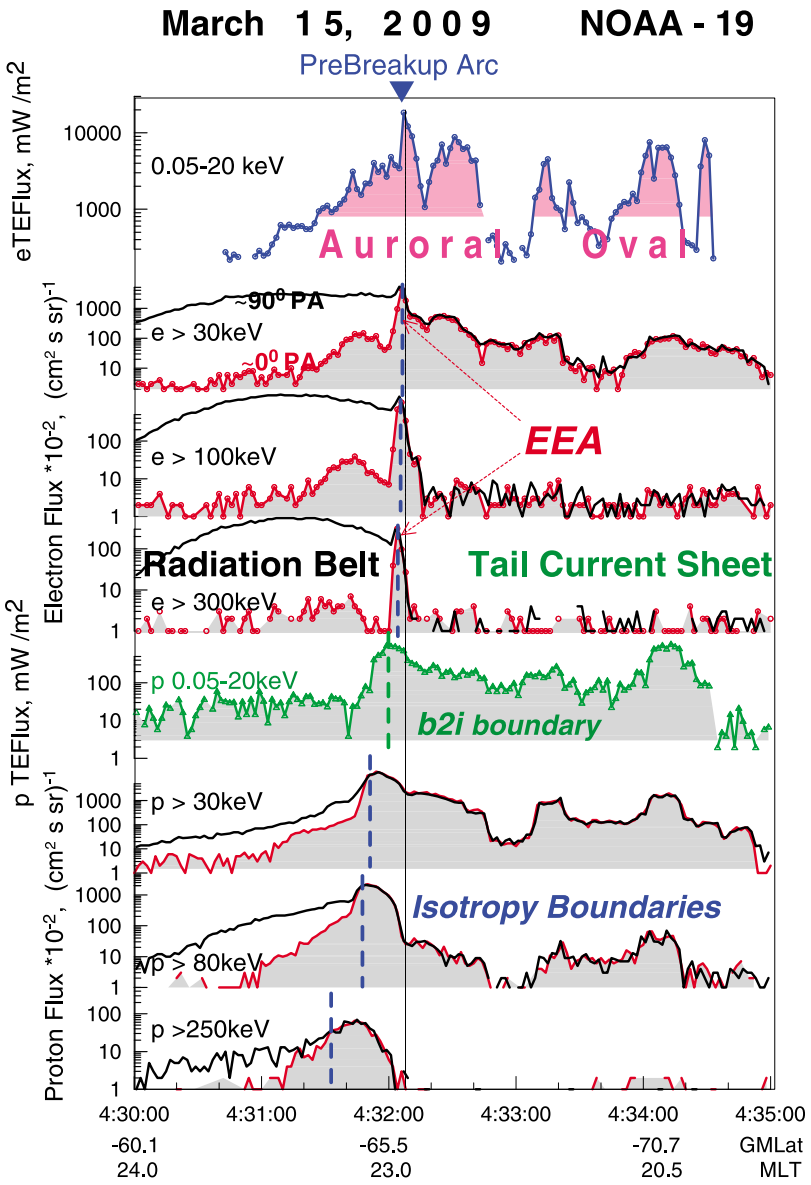

Figure 1. Particle characteristics measured by the low-altitude polar NOAA-19 spacecraft during its near-midnight pass in the southern hemisphere on 15 March 2009. Different types of regions and boundaries are marked.

the trapped (90° pitch angle) radiation belt population (black curves for electrons >30 keV).

[9] The above observations indicate that the breakup arc flux tubes are somewhere in the transition region between the dipole-like region and the current sheet region. This transition region can be quite broad (several Earth radii in the equator). One must therefore determine with higher accuracy the exact location the arc maps to, especially given the fact that the actual/ equatorial parameters (B, j, plasma pressure and plasma beta, etc.) can change very dramatically over the transition region.

[10] In this paper we address this problem from three perspectives. First, we compare the prebreakup arc (PBA), identified using ground imagers, with energetic particle profiles similar to those in Figure 1, to establish the PBA's relationship to isotropy boundaries and EEA structures. Our approach starts from a list of breakup events in 2008 and 2009 from *Nishimura et al.* [2010a], assembled from the THEMIS All-Sky Imager (ASI) [*Mende et al.*, 2008] observational data set. Using orbits of POES spacecraft mapped into the northern hemisphere, we identified sixteen PBA overpasses determined to have occurred within a few minutes of the breakup time and near the breakup location. We identified the PBA as the most equatorward arc in the nightside auroral oval whose strong brightening and structuring initiates poleward expansion of the ensuing large-scale onset. We subsequently linked the peaks in the POES satellite precipitating auroral energy flux data with the PBA. By comparing the PBA latitudes with IB locations at various energies and with the radiation belt outer boundary, we explored the consistency of our findings across multiple events.

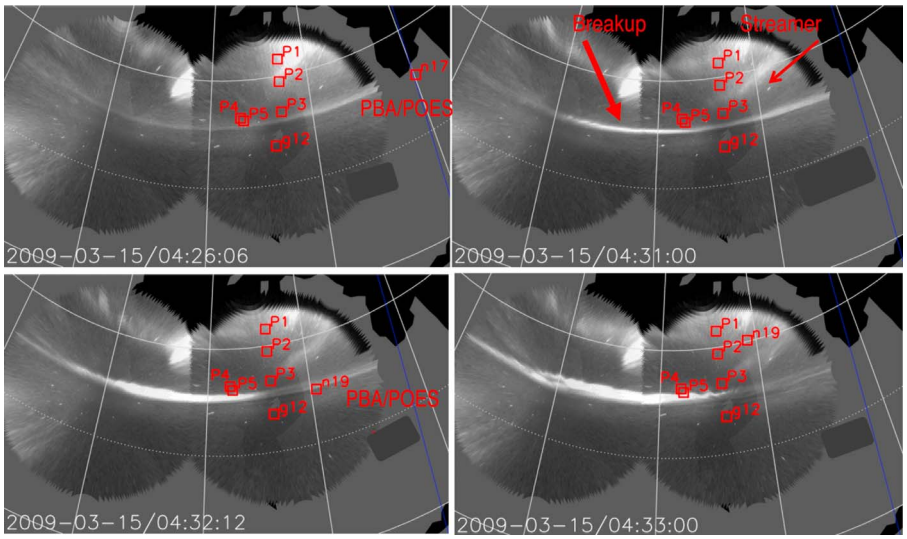

Figure 2. THEMIS ASI data during an auroral onset on 15 March 2009. ASIs used are SNKQ (to the East) and GILL (to the West). White lines are isocontours of magnetic latitude (every 10° in solid lines) and longitude (every 15°). The blue line in each image is the magnetic midnight meridian. The onset occurred at T_0 = 04:30:30 UT. The entire sequence is shown in Animation S1.

[11] Second, for the three best events (containing 5 of the above 16 crossings) we constructed adaptive magnetospheric models based on THEMIS [*Angelopoulos*, 2008] and GOES magnetic observations. We compare the observed IB locations with the model predictions to assess the model uncertainty. We then discuss the mapping of the PBA into the equatorial magnetotail, taking into account all this information.

[12] Third, the THEMIS in-situ observations of preconditioning and BBF/dipolarization features available for these three events due to our event-selection criterion designed to enable magnetic modeling, provide additional information about the dynamical magnetotail process that may contribute to the breakup. Integrating these three perspectives, we conclude by discussing the significance of our results and present an interpretation of our observational findings.

[13] In this paper we extensively use the magnetic (FGM) and plasma (ESA and SST spectrometer) observations at the THEMIS spacecraft [see *Angelopoulos*, 2008, and references therein], auroral observations at 3 sec time resolution by the THEMIS All-Sky Imager (ASI) network [*Mende et al.*, 2008], particle observations by MEPED and TED spectrometers on POES spacecraft [*Evans and Greer*, 2000], and some DMSP particle observations and magnetic observations at the GOES spacecraft.

2. Event 1: 15 March 2009

[14] During this moderate substorm event, the auroral electrojet (AE) index started from a relatively low background and reached a peak (AE > 400 nT) at about 05 UT. The growth phase was initiated by the southward IMF turning observed at around 0350 by Geotail and Cluster spacecraft just upstream of Earth's bow shock. This stimulated increases in the polar cap (PC) index and AE index after ~0400 UT (all cited data not shown here are available at http://cdaweb.gsfc.nasa.gov).

[15] The auroral dynamics in the region of interest were observed by two ASI imagers and shown in Figure 2 and in auxiliary material Animation S1.[1] The auroral breakup was identified at 04:30:30 UT. Prior to the breakup a well-resolved, thin, bright arc (the PBA) is seen in the equatorward portion of the auroral oval, extending across the fields of view of both ASI stations slightly northward of zenith. The PBA gradually moved equatorward during the growth phase. Simultaneously there was auroral activity in the northern sky that could not be well-resolved, partly because of light contamination from a nearby town.

[16] An equatorward-propagating streamer inclined by ~45° to the magnetic meridian can be discerned in the poleward sky East of the THEMIS foot point meridian. (Such streamers have been noted to initiate substorm onset [*Nishimura et al.*, 2010a] and may have associated plasma-depleted fast flow channels in the tail [e.g., *Xing et al.*, 2010]). Direct contact of this faint streamer with the equatorial arc is not clearly visible, however. PBA brightening and structuring (i.e., the appearance of rays) started after T_0 = 0430:30 UT in a ~1 h MLT-wide segment of the pre-breakup arc, just west of the THEMIS foot point meridian.

[17] Prior to breakup, the foot points of the near-Earth (~11 Re) THEMIS spacecraft (probes P3, 4, 5 – THEMIS-D, THEMIS-E and THEMIS-A, respectively) were within 1° CGLat of the PBA on its poleward side (Figure 2). P4 and P5, which had approximately the same X and Y GSM coordinates in space, were separated in Z by 0.9 Re. Throughout the event P4 and P5 stayed on opposite sides of the neutral sheet, allowing us to determine precisely the neutral sheet position and to control cross-tail current density variations. Steady current sheet thinning during the growth phase after 0408 UT can be seen by comparing B_x-component difference between P4 and P5 in Figure 3, which grows 2 times by breakup time, reaching an average

[1] Auxiliary materials are available in the HTML. doi:10.1029/2011JA017154.

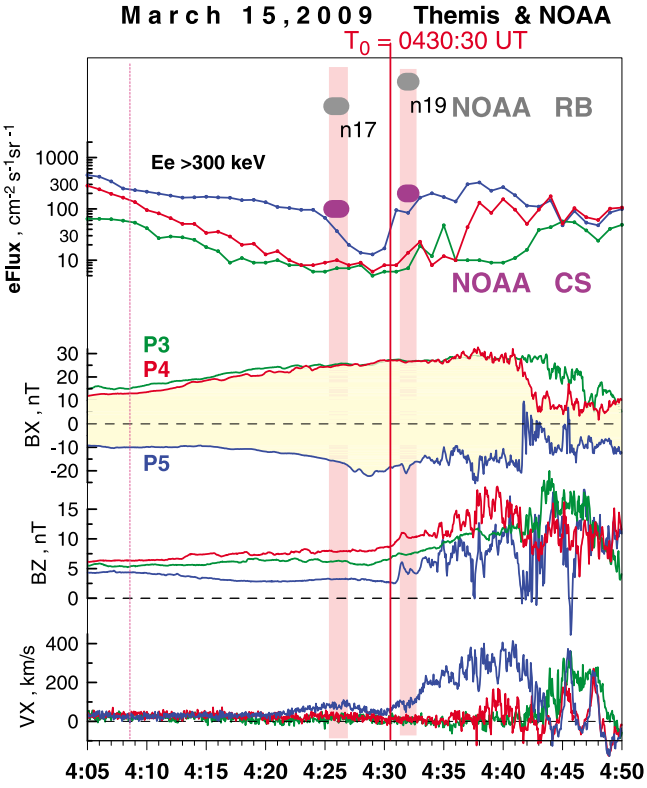

Figure 3. THEMIS observations of (top) energetic electron flux, (middle) magnetic field and (bottom) plasma flow. Vertical strips indicate time intervals of auroral zone crossings by the POES spacecraft, red vertical line marks the auroral breakup. The characteristic values of energetic particle flux in the radiation belt (RB) and current sheet (CS) are also shown in Figure 3 (top) based on low-altitude POES observations.

current density of ~8 nA/m^2. The embedded TCS in the central part of the plasma sheet may have higher density, as we will show below. By 0428 UT P3, P4 and P5 exit the central part of the current sheet and enter its northern and southern sides, respectively. P5 returns to the central part of the current sheet by the time of breakup. After correcting for current sheet tilt, the average B_z in the neutral sheet at 11 Re is 5 nT, and before breakup (not shown), the shear magnetic component is $B_y \sim -4$ nT.

[18] The energetic particle flux measured by the SST instrument is useful for comparison with low-altitude particle data, such as those shown in Figure 1. The $E > 300$ keV electron channels at P3, P4, P5 (Figure 3, first panel) show considerable flux decrease during the growth phase with subsequent recovery during the expansion phase. Because the observed variations (both spatial and temporal) are similar to variations of electron temperature and the plasma beta parameter (not shown), they can be interpreted as spatial variation related to energetic particle flux decreasing downtail. In this interpretation, an order-of-magnitude flux difference observed at three THEMIS satellites before 0425 UT and from 0431 to 0440 UT may indicate that during these time intervals, the spacecraft remain in the region of sharply decreasing particle flux, which resembles a sharp outer boundary region of the radiation belt seen at low altitudes (Figure 1). Recalling a possible strong pitch angle anisotropy, flux comparisons at low and high altitudes shown in Figure 3 (first panel) may suggest, that THEMIS spacecraft are in the region of rather low energetic particle flux. This region is located poleward of, but very close to, the sharp outer boundary of the radiation belt (and poleward of the PBA, which is consistent with mapping shown in Figure 2).

[19] During the growth phase, the midtail spacecraft (P1 and P2) are at ~17 Re in the southern part of the current sheet, mostly separated in Z by ~1 Re. They observed a 15% total pressure increase during the growth phase. Near the breakup they moved from the high-flux interior of the plasma sheet toward its outer edge. Substorm onset-related variations are thus not as dramatic at P1 and P2 because they were away from the neutral sheet.

[20] A sharp but weak ($dB_z \sim 2.5$ nT) transient dipolarization was observed at 0431 UT at P5 (closest to the neutral sheet), P4 and also a smoother dipolarization at P3. The plasma flow V_x component at P5 increased up to a few hundreds km/s after breakup time. Its gradual onset was determined to have begun after ~0430:30 UT. No comparable V_x flow increase was observed at P3, P4, until 6–10 min later. This delay is reasonable because the spacecraft were on the dawn side of the breakup in longitude, in the plasma sheet boundary layer (away from the neutral sheet). Additionally, no significant V_y was observed (not shown). The GOES 12 spacecraft, which stayed at the same longitude as the THEMIS spacecraft, but with its foot point located equatorward from breakup arc (Figure 2), observed a weak ~2 nT dipolarization signature after 0434 UT (see, e.g., Figure 4).

[21] For this event, spacecraft coverage was very useful for adaptive modeling, not only because of the good radial coverage provided by 6 spacecraft (Goes 12 and 5 THEMIS probes at distances between 6.6 Re and 17 Re, all near the ~23 h MLT meridional plane), but also because P4 and P5 bracketed the neutral sheet, enabling monitoring of the variable current sheet tilt and growth of the electric current density. Here we use the same approach as recently described by *Kubyshkina et al.* [2011]: We construct models at a 1 min time step between 0400 and 0450 UT, allowing variation of nominal tail and ring current system intensities together with the intensity and thickness of an additional current sheet (TCS) superimposed on the standard current systems of the nominal model. We also vary the tilt of the current sheet in the XZ plane. Modeling relies on minimization of the standard deviation between predicted and observed quantities (i.e., the magnetic field components at all spacecraft, and the total pressure at midtail P1 and P2) to get the best fit values of all varied parameters. Figure 4 shows a comparison of predicted magnetic fields (red) with observed magnetic fields (black) and with predictions from the standard T96 model (green) (after the International Geophysical Reference Field, IGRF, has been subtracted). The adaptive model matches the observations in time much better than the standard model. Our modeling also provides estimates of important parameters, such as TCS half-thickness (h), variations of which are also shown in the top right. These variations show current sheet thinning fairly well and provide an indication that h could reach very low values just before breakup. As a case in point, between 0428 and 0432 UT the model h dropped to 0.1

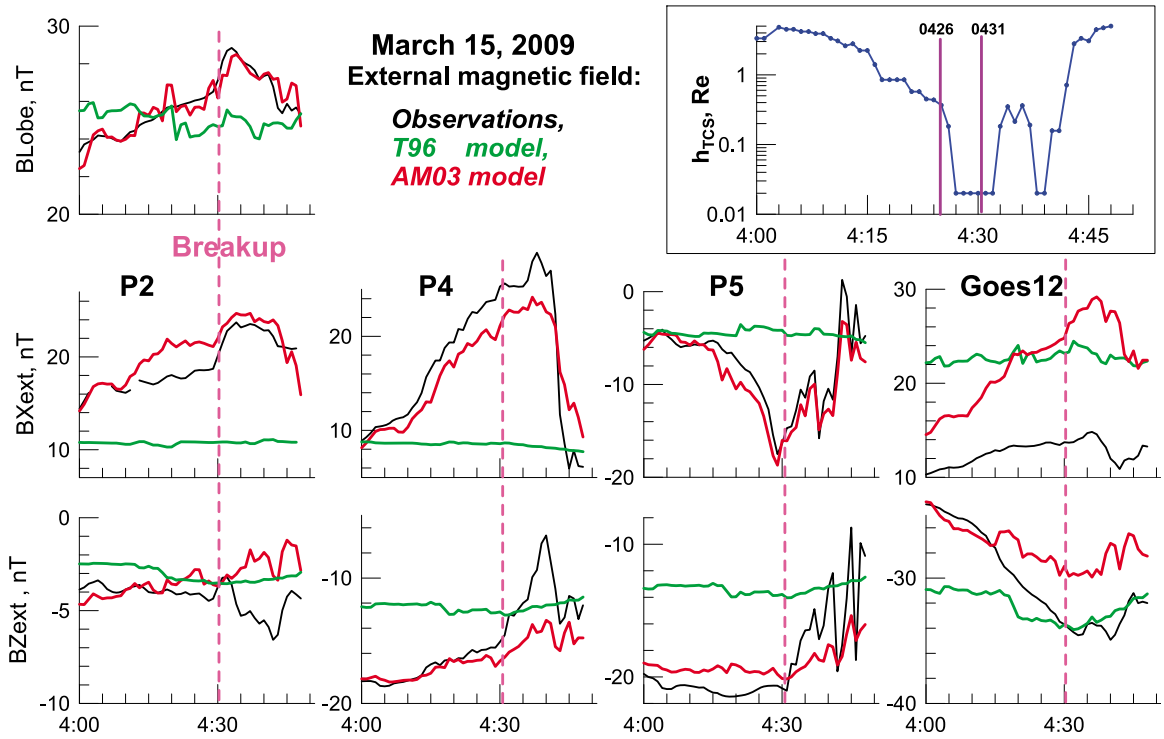

Figure 4. Comparison of observed (black) and modeled magnetic field components (adaptive and T96 model predictions are shown by red and green lines, respectively). Only the external part of the magnetic field (IGRF component subtracted) is shown here. The plot at the top right shows the variation of the thickness of the additional (thin) current sheet as follows from adaptive model.

Re (the minimal value allowed), comparable to an ion inertial length of ~500 km.

[22] The NOAA-17 and −19 spacecraft passed above the PBA along nearly the same meridian ~4 min before and ~1 min after the breakup, respectively (see Animation S1). Their observations (in the same scale and format) are compared in Figure 5. Most of these features have already been mentioned in the discussion of Figure 1 in section 1. The general pattern and location of basic boundaries are stable. We applied the adaptive model results to map POES spacecraft trajectories from the southern into the northern hemisphere. Along each modeled field line, we also computed the maximum value of the ratio Rc/ρ (for 30 keV protons), as well as the minimum magnetic field value B_{eq}. Both extrema are nominally observed at the magnetic equator. The results are shown in Figure 6.

[23] Assume that the isotropy boundary should occur where $Rc/\rho = 8$. Noting that at any point the Rc/ρ ratio for a particle of any specia/energy is scaled inversely to its rigidity G, the critical ratios for non-adiabaticity for any energies and species can be properly scaled to the reference variable ($Rc/\rho = 8$ ratio for 30 keV proton) shown on the ordinate axis of Figure 6 (bottom). These scaled critical ratios are indicated by the horizontal dashed lines in Figure 6 (bottom). Their intersections with the Rc/ρ curve show model predictions of isotropy boundary location for particular energy/specia. On the other hand, the equatorial location of the IB can be obtained by mapping the Corrected Geomagnetic Latitude of the IB observation by a POES satellite using the AM03 model. Each IB observation is then plotted as a symbol on the corresponding horizontal dashed lines (showing critical Rc/ρ values for particular energy/specia). If the adaptive model used is an accurate representation of reality, the symbols should match with the Rc/ρ curve indicating the location of the critical values predicted solely by the adaptive model.

[24] Comparison of IB latitude profiles measured at two nearly simultaneous POES satellite passes shows that they map near each other at the equator. The mapped radial IB profiles are not far from the expected locations as determined by the model (the solid lines). However, the observed profiles are considerably steeper functions of radial distance than the model predictions. The PBA locations fall at the beginning of the plateau portion of the mapping curve (latitude versus equatorial distance) shown in Figure 6 (top). That plateau forms as a result of low B_z in the current sheet region, evidenced by the THEMIS spacecraft and adhered to by the adaptive model.

3. Event 2: 11 February 2008

[25] This event occurred in a geomagnetically disturbed period (K_p = 4, AE did not fall below 200 nT during this hour), during a high-speed (~700 km/s) solar wind stream and moderately enhanced dynamic pressure (~3 nPa). There was no ordinary growth phase, an ~20 minute-long interval of southward IMF accompanied by temporary growth of AE index and by D_{st} depression, concluded by 0415 UT. However, this event is an example of very distinct fast flow burst and dipolarization onset in the conjugate equatorial region during the breakup (T_0 = 0427:08 UT) and with interesting preconditioning of magnetotail before the breakup, both

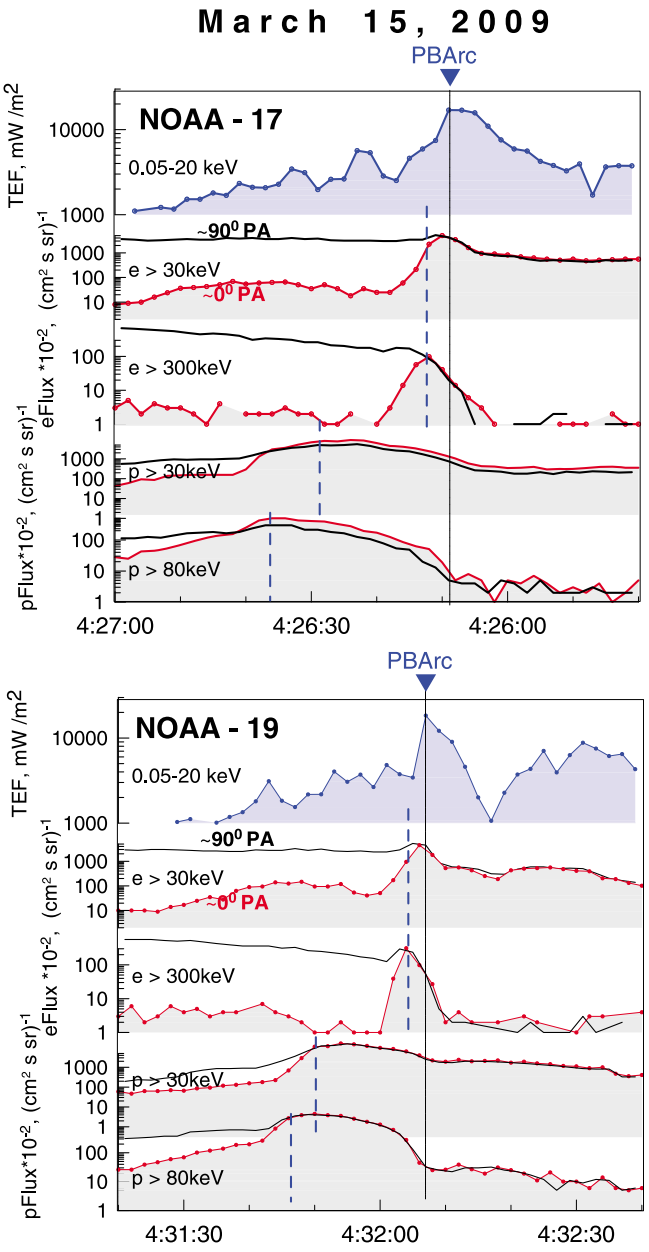

Figure 5. Energetic particle observations by two POES spacecraft made in the same MLT sector with a ~5 min time difference. Data are presented in the same scale in the vicinity of the prebreakup arc (PBArc).

observed with good coverage by the THEMIS and GOES spacecraft.

[26] Five to ten minutes before breakup, three arc systems were evident, spanning a 66–69° latitude range (see Figure 7 and Animation S2). At about 0418 UT intensification of the polewardmost auroras followed by equatorward motion was observed at 22 h MLT; that motion did not cause large distortion/disruption of the more equatorward arcs. Two minutes prior to the breakup (at ~0425 UT) a middle arc system brightened at ~67°. The arc system slightly above 65° GMLat was initially faint and diffuse. The quiet, regular equatorward arc spanned more than 3 hours MLT in longitude. Another faint arc slightly poleward of it could be seen in the sector 21–22 h MLT. This system of two closely-spaced arcs, the prebreakup arc (PBA) in this substorm, showed azimuthal striations after 0427:06 UT, with intense brightening 10 sec later (0427:18 UT), as typical for the breakup [*Donovan et al.*, 2008]. It soon resulted in poleward- (and westward- and eastward-) expanding bright auroras. NOAA-18 crossed the undisturbed portion of the equatorward arc in the poleward direction 1.5 min after onset at ~23 h MLT meridian (Figure 7), just east of the breakup auroras. The spacecraft observed (Figure 8) the familiar pattern of energy-dispersed isotropy boundaries and narrow, intense precipitation of energetic electrons. The latter occurred near the latitude of the double peak of auroral precipitation associated with the split PBA.

[27] The foot points of the inner group of three THEMIS spacecraft (P3, 4, 5) and GOES-12 were mapped near

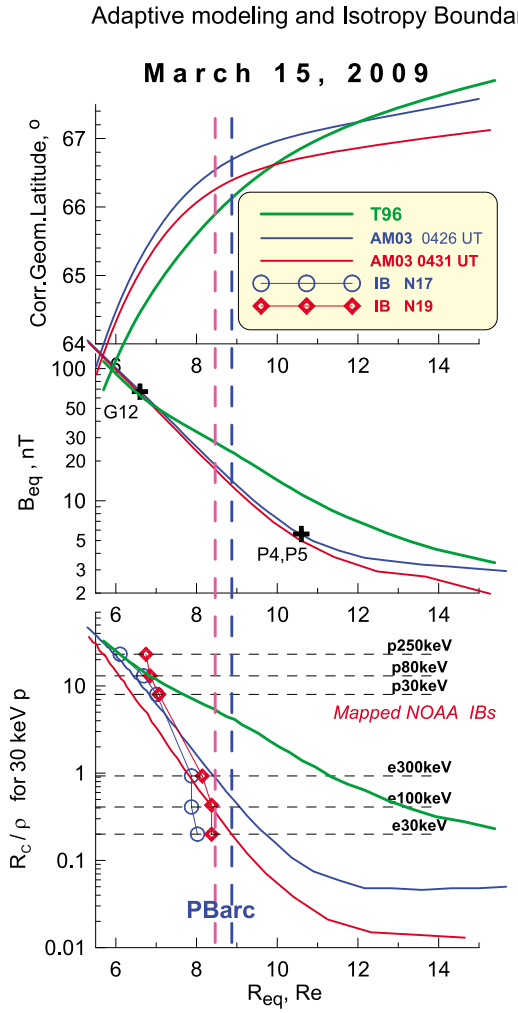

Figure 6. Model results and their comparison with observations in the flux tubes crossed by the NOAA-17 and NOAA-19 spacecraft as a function of equatorial distance in the magnetotail. (top) Corr. Geom. Latitude, (middle) equatorial magnetic field, and (bottom) R_c/ρ ratio for 30 keV protons. B_z component values in the neutral sheet at 11 Re (inferred by the interpolation between the recordings at P4 and P5) and at Goes12 are shown by crosses in Figure 6 (middle).

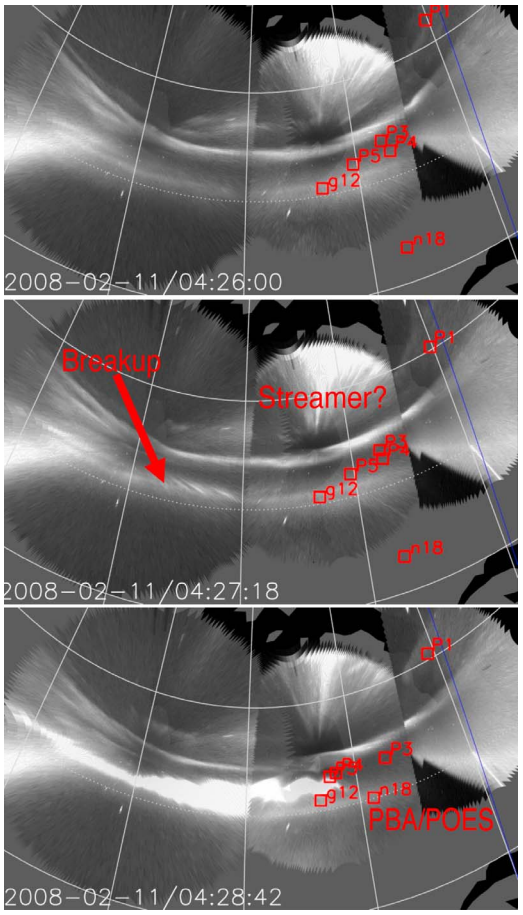

Figure 7. THEMIS ASI data during an auroral onset on 11 February 2008. The format is the same as in Figure 2. The breakup started at T_0 = 04:27:08 UT. The whole sequence is shown in Animation S2.

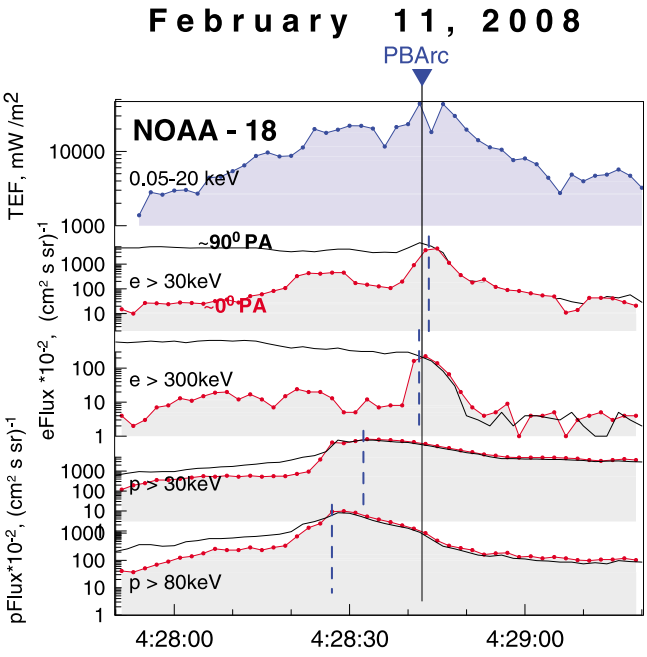

Figure 8. POES particle observations for 11 February 2008 event.

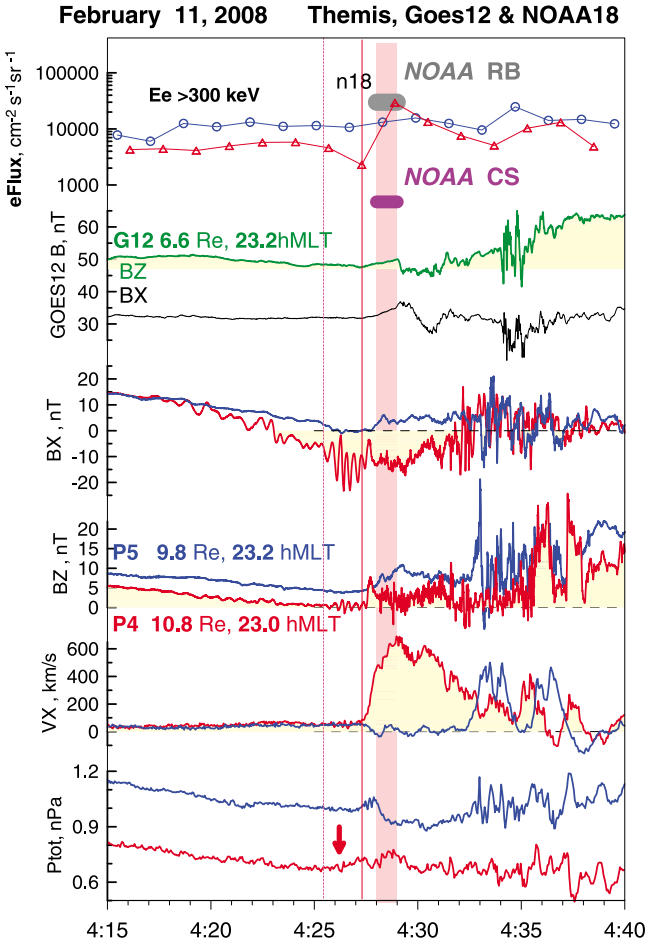

Figure 9. THEMIS and Goes12 observations of the magnetic field together with plasma flow, total pressure, and energetic electron integral flux at THEMIS spacecraft. Low-altitude values of particle flux in the radiation belt and current sheet regions are also shown according to NOAA-18 observations.

~23 MLT, slightly to the east of the initial breakup, with P5 azimuthally the closest to the breakup location. P1 probed the plasma sheet at 19 Re and 01 h MLT, and GOES 10 at 6.6 Re and 01 h MLT. Before the event, the inner THEMIS spacecraft group at around 10–11 Re observed a steady decrease in total pressure as well as a steady B_Z-component decrease – see Figure 9. P5 and P4 remained near the neutral sheet. At 0421–0423 UT, P4 (at $r \sim 10.8$ Re) crossed the neutral sheet, where it observed a small $B_z \sim 1.5$ nT and a large shear magnetic component $B_y \sim -4$ nT. P5 at $r \sim 9.8$ Re stayed in the neutral sheet between 0425:30 and 0428 UT, measuring $B_z \sim 4$ nT and $B_y \sim -4$ nT. These observations suggest that minimal B_Z of <1 nT could be located in the current sheet at around 11 Re.

[28] Interesting changes were observed during the 2 min interval preceding breakup and flow burst arrival. First, beginning at 0425:30 UT, P4 observed remarkable B_x-component oscillations with 20 nT magnitude and 20 sec periodicity that lasted until flow burst arrival. Similar oscillations but of lower strength have been observed at P3, which has a smaller plasma beta parameter and remains

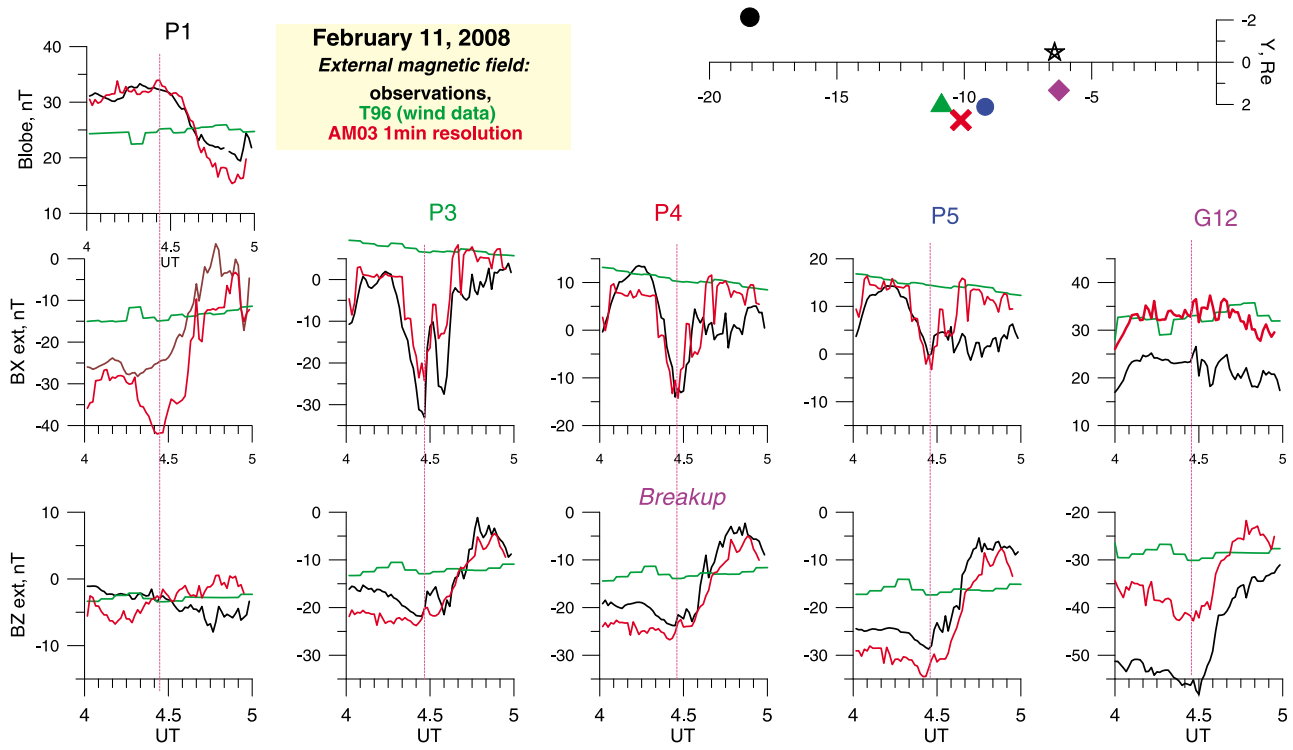

Figure 10. Same as in Figure 4 but for 11 February 2008 event. Spacecraft projections to XY plane are shown at the top right.

farther from the neutral sheet than P4 (not shown). These oscillations show a remarkable correlation between dBx/dt and the plasma flow component, V_z, or $-E_y/B_x$, the convective component, supporting their identification as vertical oscillations of the plasma sheet tubes caused by kink-type or ballooning motions. At P4 the regression coefficient between E_y/B_x and dB_x/dt is −15.5 km/nT (correlation coefficient CC = −0.96), equivalent to a very large electric current density, ∼50 nA/m^2. At P3 the regression slope is −47 km/nT (CC = −0.77) corresponding to a ∼3 times smaller current density. Surprisingly, at P5, which was only 1 Re Earthward of P4 and stayed exactly in the center of the current sheet, there were neither B_x oscillations nor comparable V_z and E_y periodic variations. This can be explained by a strongly bifurcated current (with strong minimum at P5 in the neutral sheet), a sharp Earthward termination of the thin current sheet (over ∼1 Re), or a sausage-type observed oscillation. Nevertheless, very weak B_z and a thin current sheet at an off-equatorial location at ∼11 Re are clearly demonstrated by THEMIS observations of this event.

[29] An obvious near-tail onset signature is first seen at P4. Beginning at 0427:30 UT (i.e., 20 s after breakup onset), P4 observed a strong Earthward BBF with peak flow >600 km/s in the radial direction, a moderate fluctuating B_z increase (dipolarization), and strong Earthward flux transport with E_y > 4 mV/m continuing for >3 min. P5 observed small, slightly delayed dipolarization but without such strong flux transfer. And GOES 12 began to register variations that might have been the remote signatures of activated field-aligned currents. In advance of BBF arrival, a 1 min long increase in the total pressure, marked by red arrow in Figure 9, propagated Earthward from P4 to P5. Such a compression-like, 1 min-long precursor often precedes arrival of an Earthward-moving dipolarization front and a BBF [*Dubyagin et al.*, 2010; *Zhou et al.*, 2011]. Taken together, THEMIS observations are consistent with a distant source at r > 11 Re that sends the compression and then the azimuthally-localized BBF/dipolarization toward the Earth. This source could be activated at least 1 min before breakup of the equatorwardmost arc (when the compression precursor starts to be observed) or 2–2.5 min before both the breakup and BBF arrival to 11 Re, if the earliest signatures of dramatic B_x oscillations are related to this source process.

[30] This case, with six spacecraft covering the distance from 6.6 to 19 Re in the local time sector of the breakup, is also very suitable for adaptive modeling, the results of which are shown in Figure 10. Certainly, the adaptive model performs much better than the standard model, especially in reproducing large temporal variations. The agreement in absolute values near the time of breakup is also good at the THEMIS spacecraft, whereas at GOES 12, it is not as good as in the previous event. At 6.6 Re the model underestimates the observed depression in the B_z component by as much as 15 nT, which means that actual spacecraft foot points could be at ∼1° lower latitude than those shown in Figure 7. Anyway, the equatorwardmost prebreakup arc is expected to lie between the foot points of the THEMIS and GOES spacecraft. The adaptive model did not resolve any thin current sheets.

[31] As in previous case, we mapped the NOAA-18 spacecraft trajectory from the southern to the northern hemisphere using the adaptive model and computed the maximum value of R_c/ρ ratio for 30 keV protons as well as

Magnetic Configuration and Isotropy Boundaries

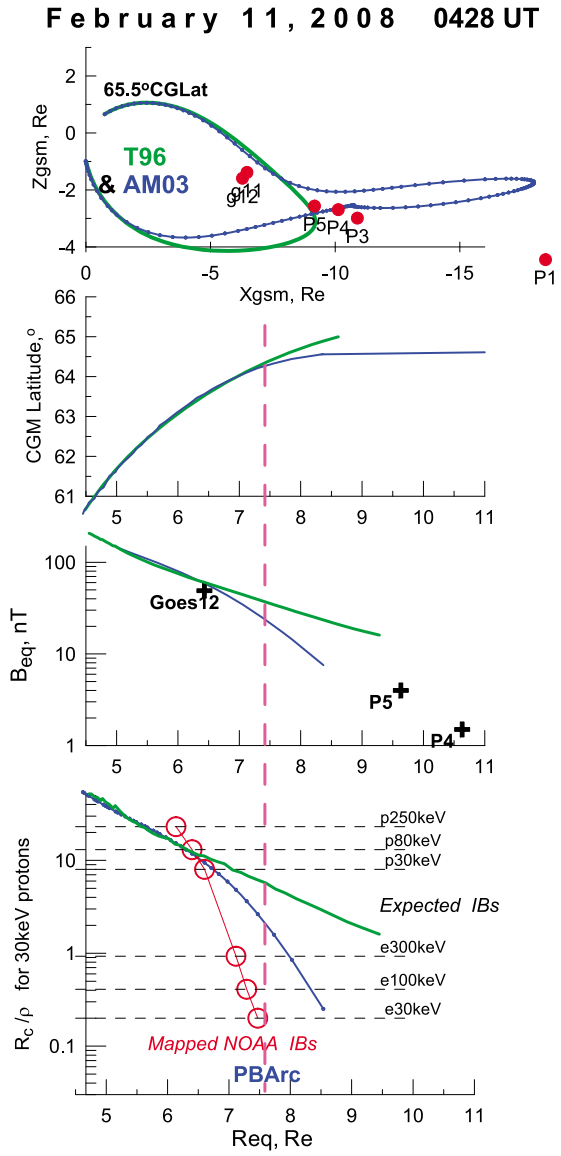

Figure 11. Same as in Figure 6 but for 11 February 2008 event. In addition, the first plot shows the field lines starting from 65.6°CGLat in the ionosphere in T96 and AM03 models, to illustrate very different field line stretching and CS tilts in two models (although both resulted in the same foot point latitude of P5 spacecraft).

the minimal magnetic field value along these field lines in the equatorial region (see Figure 11). The results are similar to the previous case. In particular, isotropy boundaries together occupy the right domain of the tail, but the observed profile is steeper than in the model prediction.

4. Event 3: 14 March 2009

[32] This was a small substorm event (AE reached a peak 200 nT by 0540 UT). It occurred during a weakly southward IMF that started at ~0430 UT under moderate (1.3 nPa) solar wind dynamic pressure. The substorm growth phase was noticeable as a small increase in the PC index and a depression in the geostationary magnetic H_p component starting at 0440 UT.

[33] THEMIS ASIs observed rayed, active arcs on the poleward side that are brighter at the westward station (GILL), as seen in Figure 12 and Animation S3. They also observed a slowly-drifting, equatorwardmost quiet arc spanning a few hours in MLT, with somewhat greater brightness toward the eastward station (SNKQ), which was near local midnight (shown as blue meridians). For 1 to 2 minutes prior to the breakup a clear auroral streamer was observed in the poleward sky of SNKQ: it propagated southwest into the area of the ensuing substorm breakup. As in the previous case, the breakup started by forming azimuthally-spaced auroral striations (at T_0 = 0505:48, at longitudes between two stations). These were soon followed by intense brightening about 50 km north of the azimuthally-extended prebreakup arc, which later resulted in auroral expansion.

[34] The foot points of the three inner THEMIS spacecraft (P3, 4, 5) and GOES-12 mapped near ~23 MLT, slightly eastward of the initial breakup. Near the sharp ground onset signature, a BBF with a small, transient B_z variation was first seen at 0506:10 UT by P5, which had a smaller plasma beta

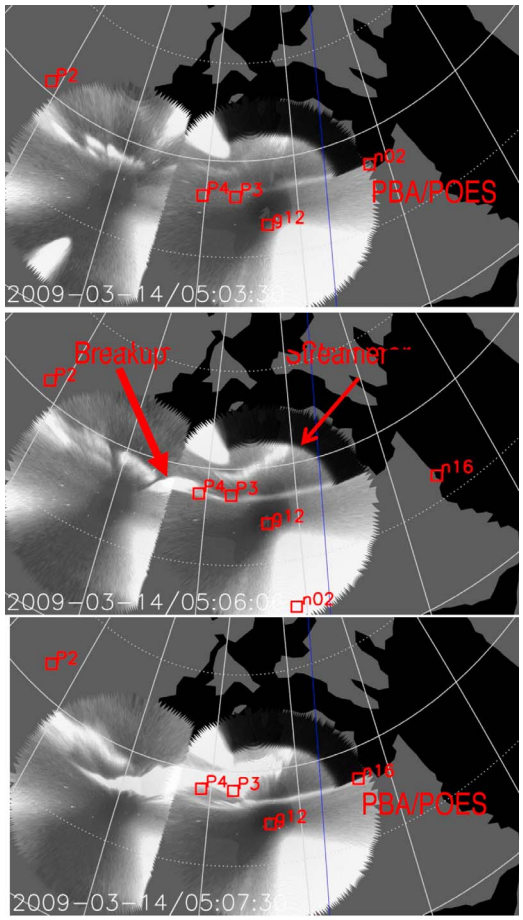

Figure 12. THEMIS ASI data during an auroral onset on 14 March 2009. The format is the same as Figure 2. The breakup started at T_0 = 0505:48 UT. The whole sequence is shown in Animation S3.

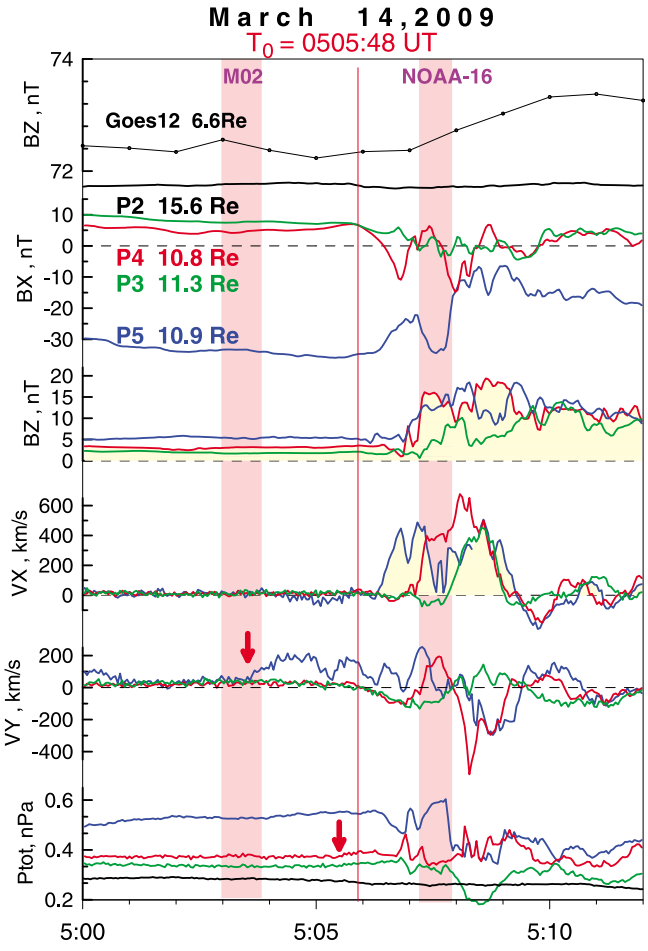

Figure 13. THEMIS and Goes12 observations of magnetic field, plasma flow and total pressure.

parameter, and therefore was farther from the plasma sheet center than P3 and P4 (Figure 13). This, together with the flow burst progression in time (P5→P4→P3) indicates the BBF's Earthward propagation into the inner region, with the dawnward flow component V_y indicating flow diversion. The final dipolarization, which also showed dawnward propagation, occurred later (after 0507 UT). As in Event 2, weak compression effects before BBF arrival were observed near the plasma sheet center (at P3, P4) from 0505:40 UT, i.e., just before the start of auroral breakup. Interestingly, the earliest indications of tail activity were observed at 0503:40 (2 full minutes before the breakup) as an increase in the V_y flow component at P5. These indications of precursor tail activity prior to auroral breakup agree with the auroral precursors mentioned previously.

[35] This event also has comprehensive spacecraft coverage in the magnetotail between 6.6 Re and 30 Re (P1), with P3, 4, 5 bracketing the neutral sheet region. As expected, the adaptive model does much better in matching the tail magnetic field observations than the standard model (see Figure 14). The fit shows a good agreement in absolute values with the observations near the time of breakup except at geosynchronous altitude (at GOES 12), where B_x is overestimated by ~10 nT. Thus, field stretching cannot be fully reproduced there. The adaptive model clearly reproduces the current sheet thinning, showing that a minimum half-thickness of 0.4 Re was reached at 0506 UT, i.e., by the time of breakup. As in other events, the prebreakup arc is located between the mapped foot points of THEMIS and GOES; it this event, however, it was much closer to the THEMIS foot point latitude.

[36] As in the first event, there were two crossings of POES-type spacecraft in the same ~0.5 h MLT sector (Figure 15), with roughly similar flux profiles and boundary locations. A single peak in the total precipitated energy flux profile corresponds to the crossing over the prebreakup arc (Figure 12), which remains near the energy-dispersed energetic electron precipitation peak. Comparison of observed and predicted equatorial isotropy boundary locations in Figure 16 again shows that the model IBs are in the approximate equatorial location of the observations, but the observed profiles are steeper than the predicted ones. It is noteworthy that the IB versus equatorial distance profiles from the two POES passes differ slightly more than on previous events. This may be partly attributed to the fact that the second POES satellite traversal was made during the expansion phase. During that time the magnetic configuration outside of the local time of the active dipolarized region (traversed by NOAA-16, 1.5 min after the breakup onset) and that inside of dipolarized region (where the observations used to construct the model are obtained) are different so the model is less suitable for NOAA-16 mapping.

5. POES Statistics and DMSP Observations of Prebreakup Arc

[37] Based on the list of auroral breakups observed by the THEMIS ASI network in 2008 and 2009 [*Nishimura et al.*, 2010a] and coordinate trajectory information for six POES-type spacecraft (NOAA-15, 16, 17, 18, 19 and Metop-2), we identified a few dozen potentially interesting conjunctions, when the POES spacecraft crossed the nightside auroral zone within a few minutes of auroral breakup. After data processing and more detailed comparison, we identified 16 events in which the mapped trajectory passed through the yet undisturbed portion of the equatorwardmost, prebreakup arc (PBA) within the field of view of the ASI imagers under good observing conditions. Six crossings were selected in the first group because they exhibited a single peak in the precipitated auroral electron energy flux versus latitude in POES records. This peak corresponded to the PBA location in ASI observations. Four such crossings (Events 1 and 3) were presented in detail in this paper. In this group the PBA arcs stayed very close to the EEA precipitation peak (average latitudinal separation was 0.14° CGLat) and the average latitudinal difference between the IB latitudes of 100 keV electrons and 30 keV protons (dIBL) was also small, 0.60°. These are the simplest objects to study.

[38] In 7 of the 16 events there were a few spikes or wide diffuse precipitation region around the expected PBA location (and near the EEA peak, e.g., Figure 8). The average difference between equatorward peak and the EEA was 0.26° (twice as large as the events presented here), and dIBL ≈ 0.82°. In auroral observations this group of seven mostly exhibits either an arc system or more structured precipitation (as we saw in Event 2). Only 3 cases showed no clear prebreakup arc activity and no obvious peak in the precipitated

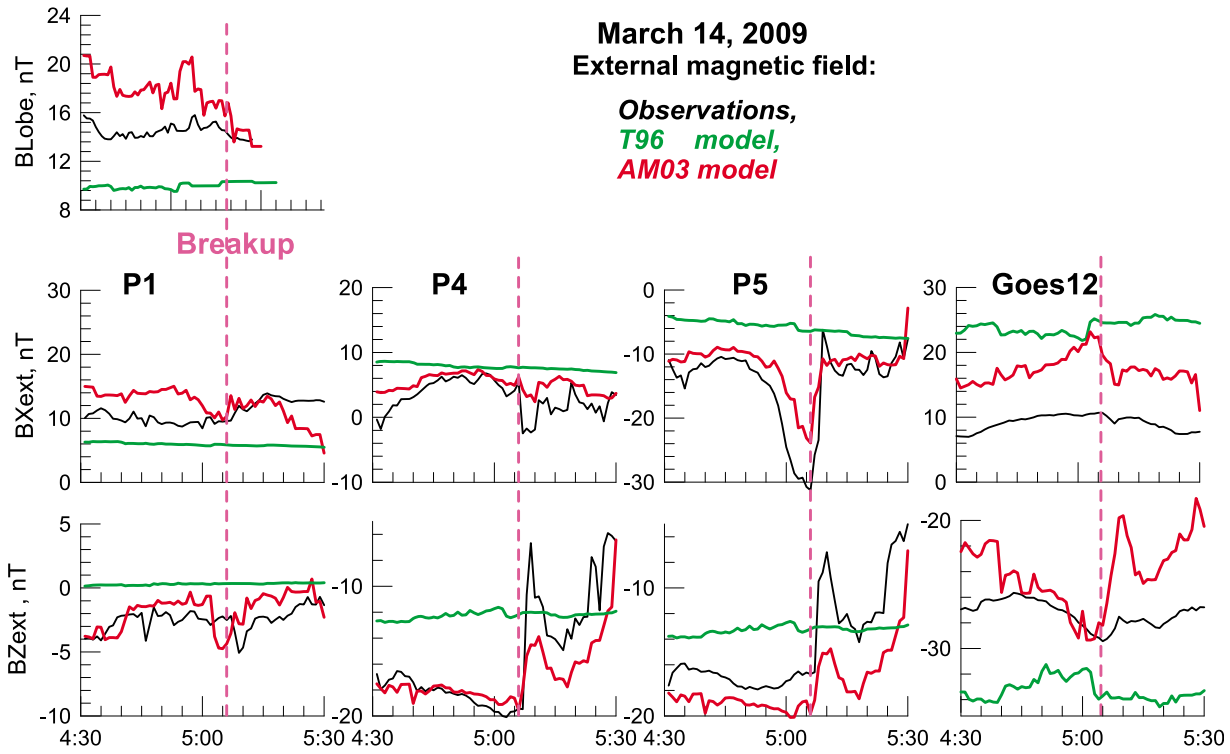

Figure 14. Comparison of observed (black) and modeled magnetic field components. The format is the same as in Figure 4.

energy flux profile within ~1° from EEA, for this group dIBL ~ 0.78°. All events demonstrate a small (only 1–2 time steps, or 2 to 4 sec between peaks 30 and 300 keV electron flux) but systematic energy dispersion of the electron isotropy boundary, with low energy electron IB staying poleward of high energy IB, as shown in Figures 5, 8, and 15.

[39] POES spacecraft do not transmit particle spectra to the ground. However in two events there were crossings of the equatorward arc by the DMSP F17 spacecraft, which provided information about such electron spectra. The bottom spectrogram in Figure 17 is centered on the time (050300 UT) during event 3, when the spacecraft foot point crossed the equatorwardmost arc. Only 30 sec later the Metop02 spacecraft (see Figure 15) crossed exactly the same structure in the same place (with <2° difference in GEO longitudes at the same latitude). In the middle spectrogram in Figure 17 DMSP crossed the equatorward arc 1 min before NOAA-18 crossing (shown in Figure 6), but this took place ~2 h MLT east of POES crossing. In both cases the electron spectra show a narrow (~10 sec long, or ~50 km wide), inverted V structure with relatively low peak energy, about 2 keV and 3 keV, respectively, remaining at the poleward edge of diffuse electron precipitation. An important fact is that near the center of this structure the fluxes in the highest energy channels (10–30 keV) show a clear peak marked by the triangle in Figure 17, which resembles the >30 keV flux peak of precipitating electrons observed by POES spacecraft (energetic electron arc, EEA). Taken together, two presented DMSP crossings confirm that the narrow prebreakup arc is associated with both field-aligned electron acceleration (inverted V) and enhanced precipitation of radiation belt electrons above 10–30 keV (EEA) that remain in nearly the same region.

6. Discussion

6.1. Observed and Adaptive Model IB Comparisons and Equatorial Location of PBA

[40] The main observational result of our study is the collocation of the prebreakup arc and the latitudinally-narrow (20–50 km) region of energetic electron precipitation. Our observations indicate that the PBA is located on the poleward side of the EEA. The EEA is a long-known feature of growth phase, recognized in ionospheric (e.g., EISCAT radar and riometer) observations [*Kirkwood and Eliasson*, 1990; *Jussila et al.*, 2004], as well as stratospheric X-ray balloon observations [e.g., *Pytte et al.*, 1976]. The relative locations of the PBA and EEA are consistent with previous work by *Sergeev et al.* [1983b], as well as previous EEA observations by *Kirkwood and Eliasson* [1990] and *Jussila et al.* [2004]. Their association with the energetic electron isotropy boundary was discussed in the paper by *Sergeev et al.* [1990], which provided the first evidence about the appearance of a thin (0.1 Re scale) current sheet in the near-Earth region just before the substorm onset. The general property of the discrete auroral arcs to be located poleward of the electron isotropy boundary has been statistically demonstrated by *Yahnin et al.* [1997], who compared POES particle observations with all-sky camera observations, but without any restriction on substorm phase and activity level.

[41] Data from five POES crossings over the prebreakup arc presented in Figures 1, 5, 8, and 15 show a typical

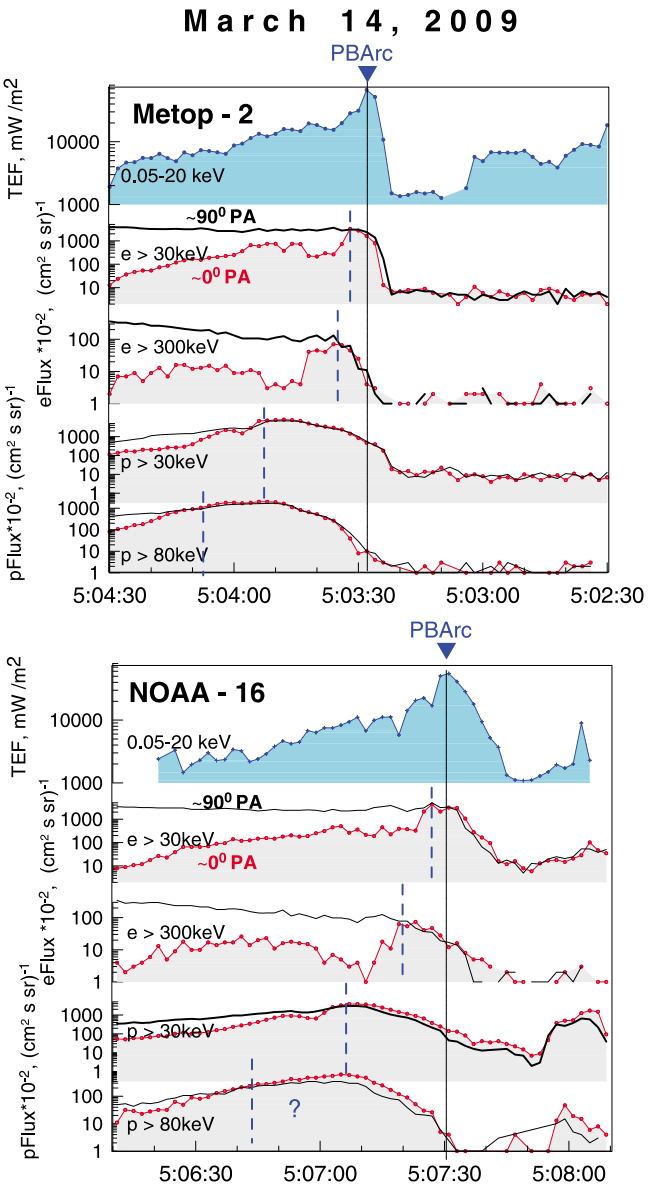

Figure 15. POES particle observations for the 14 March 2009 event.

energy/species-dependent (rigidity-dependent) pattern of isotropy boundaries previously established, e.g., by *West et al.* [1978], *Imhof et al.* [1979], and *Sergeev et al.* [1983a, 1993]. Therefore a standard interpretation of them as rigidity-dependent boundaries between regions of adiabatic and non-adiabatic particle motion is also assumed to be valid for this particular magnetospheric state. Taking advantage of available adaptive models, we compared model-predicted IB positions with observed ones in the bottom plots of Figures 6, 11, and 16 (referred to as IB profiles for brevity). Results are similar for all 5 analyzed POES crossings: the electron and proton isotropy boundaries occupy the right domain of the tail, so the models confirm the aforementioned interpretation. However, the observed profile in every case is much steeper than the model prediction. This is true for both the radial (latitudinal) separation of proton and electron boundaries and the separation between IBs of lowest (30 keV)- and highest (300 keV)-energy electrons. The electrons are of special interest here because their IB and associated narrow precipitation region (EEA) are very close to the prebreakup arc: on average the latitudinal separation between PBAs and EEAs is only 0.14° to 0.26° CGLat (or 15 to 30 km) for the PBA crossings described in section 5.

[42] Adaptive models do a much better job in describing the magnetic configuration than standard models (see Figures 4, 10, and 14), and standard models are certainly inappropriate for mapping during the time periods both before and after substorm onset. Adaptive models are not perfect, however. Here we discuss additional changes that may bring adaptive models into better agreement with

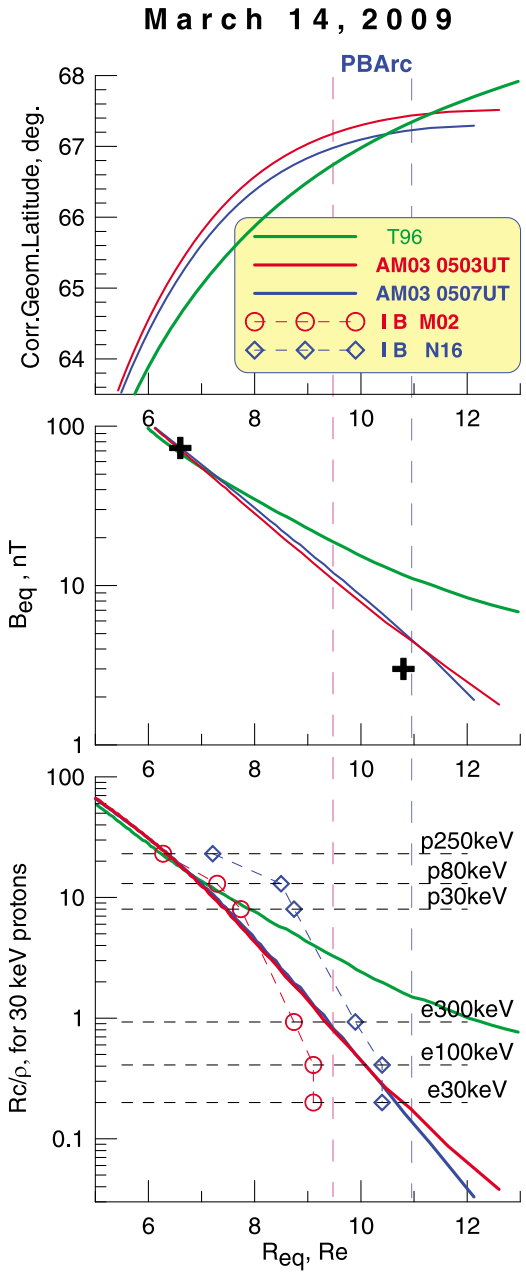

Figure 16. Same as in Figure 6 but for the 14 March 2009 event.

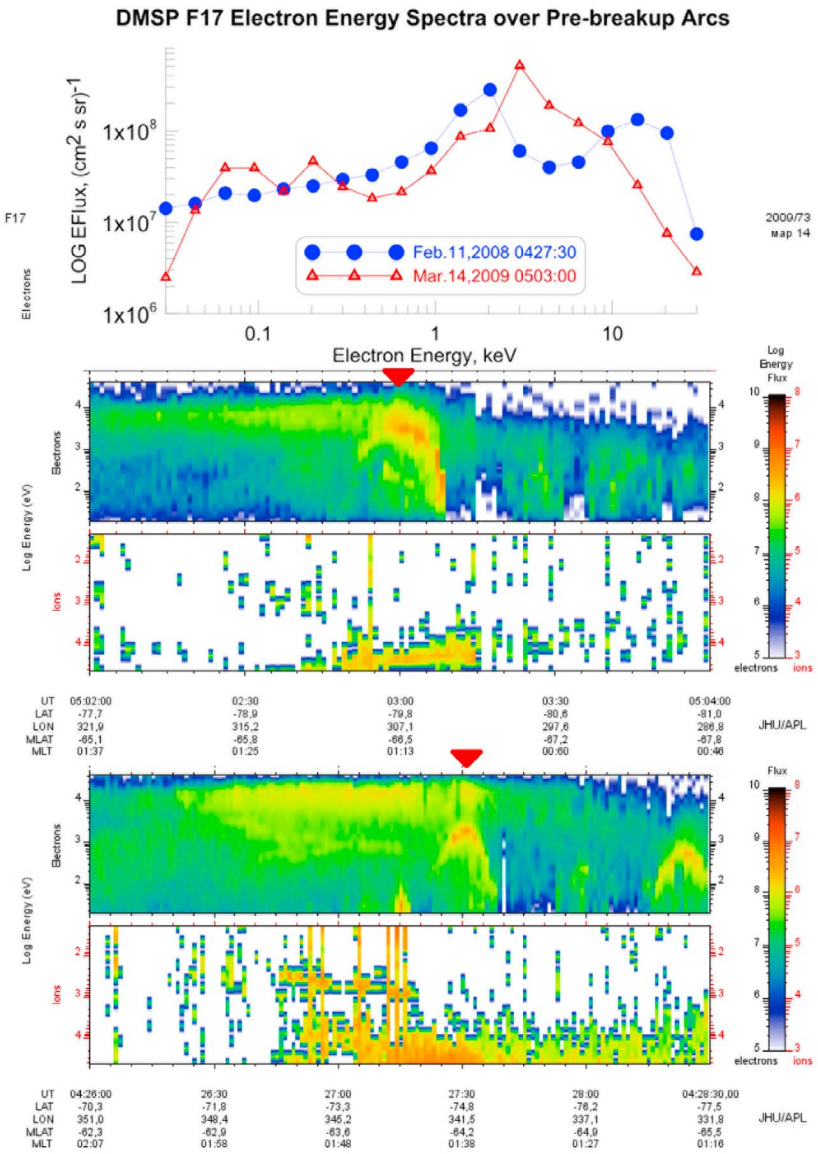

Figure 17. DMSP F17 electron and ion spectrograms during the crossings of prebreakup arc in events 2 and 3. Location of EEA is marked by triangle. Figure 17 (top) presents differential electron energy flux spectra in the PBA peak region.

observed IB locations. The criterion to get the isotropy boundary in the equatorial region is $R_c/\rho = B_z^2(dB_r/dz * G)^{-1} = K_{cr}$. The value of K_{cr} (in all available trajectory computations known to us) is usually taken to be between 6 and 10. The reader is reminded that our analysis has been done using K_{cr} = 8. This small uncertainty in K_{cr}, about 25%, cannot explain a large discrepancy between observed and predicted IB profiles, often exceeding an order of magnitude for electrons (e.g., Figure 11, blue profile in Figure 6, red profile in Figure 16). One possibility for bringing the modeled IB profiles into better agreement with observations is to suggest a larger magnetic field (B_z) gradient in the region where the electron IBs are expected (somewhere in small region between two points at 6.6 Re and 11 Re, where we have in situ observations). Another option is to introduce a thin current sheet, i.e., to increase the dB_r/dz term, but to do it only at distances where the electron IB is situated. Although modifying the radial distribution of B_z in high-beta region looks reasonable, it cannot be checked at the moment. On the other hand, a thin current sheet in the outer portion of transition region, consistent with some observations made at 11 Re, can provide the required modification.

[43] Indeed, in all three events considered, we find signatures of current sheet thinning and/or growth of an embedded thin current sheet. These signatures vary from case to case, however. In events 1 and 3 the difference in B_x-components at P4 and P5 separated by 0.9 Re in Z was growing on about a ten-minute time scale, suggesting overall thinning of the plasma/current sheet. In addition, during event 1 the adaptive model confirmed gradual, modest

Table 1. Prebreakup Arc and 30 keV e IB Parameters in the Equatorial Plane

		Equatorial Distance		Equatorial Magnetic Field		
Date	UT	R_{PBA}^{map}	R_{e30}^{mod}	B_{PBA}^{map}	B_{e30}^{mod}	B_z Goes12
150309	0426	8.9 Re	9.6 Re	16 nT	9 nT	68
150309	0432	8.4 Re	7.9 Re	18 nT	25 nT	67
110208	0428	7.5 Re	8.1 Re	24 nT	11 nT	49
140309	0503	9.5 Re	10.5 Re	10 nT	5 nT	71
140309	0507	11.3 Re	10.5 Re	3.5 nT	6 nT	71

thinning on the aforementioned timescale, but also indicated fast growth (a few minutes scale) of a very thin current sheet (see Figure 4, top right). During the third event, however, the adaptive model failed to resolve any thinning feature; the difference between events 1 and 3 could be due to fine details in the spatial coverage of P3, P4, P5 with respect to the neutral sheet. During event 2 there was no signature of modest growth-phase thinning, possibly because the IMF had turned northward 20 min before onset. Yet extremely high current densities, up to 50 nA/m^2, typical of ion gyroscale-size sheets were apparent at P3, P4 during a 2.5 min-long period of flapping oscillations preceding arrival of the fast flow burst at substorm onset. A similar observation of flapping oscillations preceding arrival of flow burst-related transient dipolarization has been reported by *Nakamura et al.* [2009].

[44] After these comments, which also illustrate the possibilities and uncertainties of adaptive models, we discuss model predictions concerning the magnetospheric location of the prebreakup arc, one of the central questions in our study. By mapping the PBA location observed at POES spacecraft to the equatorial (minimal B) region along adaptive model field lines, one gets an estimate of the equatorial distance (R_{PBA}^{map}) and corresponding magnetic field (B_{PBA}^{map}). Another useful point is the location of the 30 keV electron IB in the neutral sheet ($B_r = 0$) plane of the adaptive model according to the criterion given above (R_{e30}^{mod} and B_{e30}^{mod}). This can also serve as a proxy for the PBA location because this IB always remains close to the PBA in low-altitude observations. These parameters, together with the magnetic field at Goes12 as a measure of magnetic configuration stretching in these events, are collected in Table 1. A robust result, one of the main conclusions of our study, is that a typical range of PBA locations in the magnetosphere is roughly between 8 and 10 Re, closer to the Earth for a more stretched configuration. This is also supported by an order-of-magnitude comparison of energetic particle flux at THEMIS (see, e.g., Figures 3 and 9) with its value at POES spacecraft. In both cases the value of particle flux at 11 Re lies in between its values in the current sheet region and in the radiation belt (which differ by ~3 orders of magnitude), whereas the fluxes are at radiation belt level in the place where the PBA is situated. Thus, the flux comparison confirms that the PBA is located considerably closer to the Earth than the THEMIS spacecraft.

[45] Although the equatorial distance of the PBA magnetic field line is interesting, a more important physical parameter is the equatorial magnetic field value, which basically determines the plasma beta parameter. Its values at the PBA field line are within 5 to 20 nT range, again, increasing as the stretching of the tail configuration increases. This is already in the dipole-like region in the sense that a systematic Earthward B-gradient is present, but a plasma beta parameter value is high here (above 5–10 according to rough estimates), showing that plasma is capable of modifying the ambient magnetic configuration very strongly. Notably, according to calculations by *Cheng and Zaharia* [2004], this region is suspected to be favorable for ballooning instability.

6.2. Characteristics of the Equatorwardmost PBA and Its Possible Generation Mechanisms

[46] As reflected in the *Akasofu* [1964] substorm scheme, the auroral breakup often starts as a sudden brightening of the equatorwardmost preexisting arc, either a long-standing growth-phase arc or the arc formed a few minutes prior to onset [e.g., *Lyons et al.*, 2002; *Liang et al.*, 2008]. However, in some cases no prebreakup arc is seen, or the new arc appears poleward of preexisting arcs [e.g., *Liang et al.*, 2008; *Zou et al.*, 2010]. Although the development of the auroral breakup may show significant variations from case to case, the activation of a preexisting equatorward arc seems to be the most typical scenario.

[47] Previous observations of particle spectra and electromagnetic field above the breakup-associated arc have been made. All available particle spectra (Figures 17 (top) and 17 (bottom) and those reported by *Dubyagin et al.* [2003], *Yago et al.* [2005], *Zou et al.* [2010], and F. Jiang et al. (In-situ observations of the "preexisting auroral arc" by THEMIS all sky imagers and the FAST spacecraft, manuscript in preparation, 2012)) agree that the middle-size (tens of kilometers wide), inverted V structure with peak energy 1–3 kV is associated with the prebreakup arc or brightening breakup arc. The most detailed observations provided by FAST spacecraft near midnight over the thin (16 km) equatorward arc during its initial brightening showed [*Dubyagin et al.*, 2003], that it was associated with the inverted V structure of 2 keV peak situated in the upward field-aligned current. This equatorward breakup arc remained at the poleward edge of electron diffuse precipitation (exactly as in Figure 17) about 0.4° poleward of the b2i boundary (similar to what is shown in Figure 1). Its mapping gave the equatorial distance ~8 Re when using the standard model, which (occasionally) provided the correct estimate of the proton isotropy boundary location. These characteristics are consistent with our results. In addition, they showed that the arc-associated narrow upward FAC sheet was surrounded by downward FAC sheets and had an intense spike of southward E field situated on the poleward side of the arc, which is typical for postmidnight arcs.

[48] Important characteristics of the prebreakup arc are its lifetime (before the breakup) and its azimuthal scale. *Lyons et al.* [2002] studied the morphology of the prebreakup equatorward arc using ground auroral observations and concluded that a thin equatorwardmost breakup arc frequently appears several (2–8) minutes prior to its breakup followed by auroral expansion. They also noticed that the PBA intensity often increases slowly before breakup-associated explosive brightening. This description is consistent with what we observed in our events (see, e.g., Animations S1–S3). Concerning the longitudinal scale, the

PBA arc is often seen over the more than 2–3 hours of magnetic local time coverage of available pairs of ASI cameras, which means its azimuthal scale can be as large as >2000 km in the ionosphere. In some cases (e.g., our event 1) this thin arc looks highly regular and homogeneous over such large distances, which is remarkable and important for the following discussion.

[49] Although the origin of the longitudinally-extended (often spanning premidnight to postmidnight), narrow, equatorward auroral arc is an interesting topics by itself, to our knowledge, there is no convincing and accepted theory to explain it. Its importance is even more strengthened by its close spatial relationship to the ensuing auroral breakup (auroral image of explosive process in the magnetotail). However, the prebreakup arc is a much simpler object than the breakup and the subsequent bulge aurora. It exists for several (up to tens of) minutes, extends azimuthally over a few hours of local time, and often shows a regular behavior (simple shape, no distortions, no large brightness variations, etc), as seen during event 1. Thus, it should have a simple explanation that operates over an extended region in the magnetosphere.

[50] The close association between the PBA and the EEA provides a simple explanation for the geometric properties and regular character of the arc. Indeed, the boundary between regions with adiabatic and nonadiabatic particle motion always exists and spans a wide range of local times at nightside. The boundary should approximately follow the line of $B_{eq} \sim$ const in the neutral sheet ($B_r = 0$) plane, because B_z^2 is the main factor controlling isotropy boundary formation. This explains the east–west alignment and regular character of the EEA in the ionosphere. As dictated by the B_z depression and current sheet thinning noted, the EEA intensity should increase during the growth phase, because the isotropy boundary moves Earthward into the radiation belt region, where high particle fluxes are available. Further increase can be stimulated by an increasing slope of $B_z^2/j(r)$, e.g., due to intrusion of the thin current sheet into the outermost part of the strong magnetic field region, which would result in focusing the precipitation peaks of different energies into narrower latitudinal widths. In principle, the EEA precipitation itself can provide a weak narrow arc; however, the observations of an inverted V structure, which provides the main energy flux contribution at the location of the PBA suggest that the PBA also involves the ionosphere-magnetosphere interaction.

[51] To first order this can be understood as a result of polarization of a "seed arc" provided by energetic electron precipitation, leading to the formation of associated field-aligned current (FAC) sheets. In the presence of a westward electric field in the nightside auroral zone, a Cowling–channel develops. Here the polarization of the electrojet creates an upward FAC sheet on the poleward side of the "seed arc", which explains the observed poleward shift of the PBA location with respect to the EEA (the average shift was small, 15 to 30 km). In the presence of a meridional *E*-component this FAC configuration may vary. The scale-size of the inverted V over the PBA (about 50 km, Figure 17) is expected to be roughly of the order of the electrostatic scale length of the MI coupling [e.g., *Paschmann et al.*, 2003] or comparable to the width of EEA, which are also of the order of several tens of kilometers.

6.3. On Breakup Location, Preconditioning, and Triggering

[52] Although the focus of our paper is on the location and physics of the prebreakup arc, we briefly discuss here a few observations that which can be useful in subsequent analysis of the more complex problem of substorm onset mechanisms and the auroral breakup. In that regard, a few new auroral and magnetospheric observations are noteworthy:

[53] First, with regards to breakup triggering by the BBFs: In two of three cases studied in detail above, one of the THEMIS spacecraft at 11 Re observed a sudden increase in the Earthward flow (to >600 km/s at P4 in the event 2, and to >400 km/s at P5 in the event 3). However, these flows started ~0.5 min after breakup time. Also, in both cases the flow burst did not penetrate to the more inward spacecraft (P5 in event 2 and P4, P3 in event 3) until a few minutes later.

[54] Both observations suggest that either the BBF is very structured (so its core part was missed), or that the high-speed flows themselves may not be the immediate cause of the active processes that develop near the PBA magnetic shell, situated Earthward of the THEMIS spacecraft. However, the well-known precursor of the flow burst [*Dubyagin et al.*, 2010; *Zhou et al.*, 2011], the Earthward propagating compression in front of the flow burst, is very prominent in event 2, and it may also be discerned in the event 3 (both are marked by arrows in Figures 9 and 14). These compressions are not so localized as the fast flow bursts are, and they arrive at the periphery of the dipolelike region 0.5–1 min before the breakup. As shown in a case study by *Li et al.* [2011], such Earthward-traveling compression decreases the preexisting outward pressure gradient force. Therefore this effect potentially may destabilize the existing equilibrium and bring the system toward an instability such as the one recently discussed by *Raeder et al.* [2010]. In this context, it is interesting that, in the case of multiple auroral streamers (possibly reflecting multiple localized BBFs in the tail) observed during the growth phase, *Nishimura et al.* [2010b] found that every streamer had an associated intensity increase of the equatorward arc (they called it the growth phase arc), even though only the last one resulted in full-scale breakup. This observation nicely illustrates both the close association of BBFs with changes in the PBA region and the need for inner magnetosphere preconditioning. These results, if confirmed by a statistical analysis, may restrict the range of potential breakup trigger mechanisms.

[55] Second, concerning breakup preconditioning: Since *Lui and Burrows* [1978] (see also section 1) it is known that the location of the breakup region appears to be between the dipole-like region and the current sheet. However, location, scale-size and configuration of this broad transition region dramatically changes in the course of a substorm, and these changes are very little studied based on in situ observations. Our analysis provides evidence that near substorm onset time the breakup arc is situated in a very peculiar place, at the outer edge of a "magnetic wall" region, i.e., a region where the strong *B*- and pressure gradients are immersed within a high-beta plasma in the presence of a thin current sheet. The quantitative, although indirect, measure of the gradients in this peculiar region is provided by the isotropy boundary profiles ($R_c/\rho(r)$, shown at the bottom of Figures 6,

11, and 16) and by statistical data presented in section 5. Specifically, these data show that the latitudinal difference between isotropy boundaries of 100 keV electron and 30 keV proton is as small as dIBL $\sim$ 0.6…0.8 deg, which is a few times smaller than in average conditions. Our analysis shows that standard models are highly inadequate for describing this region, and that even adaptive models provide too smoothed an inward gradient. Future modeling efforts need to use the isotropy boundary resource to more closely reproduce the complex structure of this region, which is necessary to analyze local plasma instabilities quantitatively.

7. Conclusions

[56] Using two complementary methods, namely, diagnostics of the magnetosphere based on energetic particle observations and time-dependent data-based adaptive magnetospheric modeling, we addressed the magnetospheric location of the pre-breakup auroral arc (PBA), from which (or from the close proximity of which) the auroral breakup starts to develop. In the ionosphere the PBA was found to stay just poleward of a latitudinally-narrow, energy-dispersed precipitation band of energetic electrons, the energetic electron arc (EEA), that is centered at the electron isotropy boundary. The narrow inverted V precipitation has been found to contribute to the pre-breakup arc together with high-energy (EEA) precipitated energy flux. We suggest that EEA precipitation provides the "seed arc" whose polarization in the presence of magnetospheric convection leads to formation of field-aligned current sheets and to the growth of an inverted V in the upward field-aligned current.

[57] In the magnetosphere, the PBA location was inferred to occur at distances between 7.5 Re to 10–11 Re (depending on the amount of tailward stretching of the magnetotail), in the high-beta region at the very periphery of the dipole-like magnetosphere, where the magnitude of the equatorial magnetic field is as small as 5 to 20 nT and the inner edge of the thin current sheet can intrude. Therefore, those breakups, which start their explosive development exactly from the pre-breakup arc, are expected to be initiated in this high-beta, strong magnetic gradient "magnetic wall" region, located at the sharp interface between the dipole-like and current sheet regions. However, if the breakup starts from an arc formation somewhat (a few tens of kilometers) poleward of the main PBA (such as in Events 2,3, for example), the breakup may potentially be mapped to the neutral ($B_Z \leq 1$ nT) current sheet region, which is not very accurately resolved by even the best available adaptive models. Currently the question of the exact breakup location in space can not be fully resolved based on mapping techniques alone.

[58] In two of three cases the THEMIS spacecraft observed sudden growth (intrusion) of a fast flow burst, which started $\sim$0.5 min after breakup time so it could not be the immediate reason of the breakup developing in 8–10 Re region. However, the flow precursors, namely, $\sim$1 min long pressure enhancements, were detected $\sim 0.5 - 1$ min before the start of breakup and they could possibly participate in destabilizing the dipole/tail interface region. The details of the breakup-triggering process still need a more detailed and systematic observational study.

[59] **Acknowledgments.** The DMSP particle detectors were designed by Dave Hardy of AFRL, and data obtained from JHU/APL. CDAWeb database is run by the NGDC at NASA/GSFC. Thanks to K. H. Glassmeier, U. Auster, and W. Baumjohann for the use of FGM data provided under the lead of the Technical University of Braunschweig and with financial support through the German Ministry for Economy and Technology and the German Center for Aviation and Space (DLR) under contract 50 OC 0302. We thank L. Lyons, T. Sotirelis and N. Tsyganenko for the discussions, and M. Kholeva and Judy Hohl for help in preparing the manuscript. The work was supported by THEMIS contract NAS5-02099. The work by V.S. and M.K. was also supported by SPbU grant 11.38.47.2011, by FP7 grants 269198 (Geoplasmas) and 263325 (ECLAT), and by RFBR grant 10-05-91163.

[60] Masaki Fujimoto thanks the reviewers for their assistance in evaluating this paper.

References

Akasofu, S.-I. (1964), The development of the auroral substorm, *Planet. Space Sci.*, *12*, 273–282, doi:10.1016/0032-0633(64)90151-5.

Angelopoulos, V. (2008), The THEMIS Mission, *Space Sci. Rev.*, *141*, 5–34, doi:10.1007/s11214-008-9336-1.

Angelopoulos, V., et al. (2008), Tail reconnection triggering substorm onset, *Science*, *321*, 931–935, doi:10.1126/science.1160495.

Cheng, C. Z., and S. Zaharia (2004), MHD ballooning instability in the plasma sheet, *Geophys. Res. Lett.*, *31*, L06809, doi:10.1029/2003GL018823.

Delcourt, D. C., J.-A. Sauvaud, R. F. Martin Jr., and T. E. Moore (1996), On the nonadiabatic precipitation of ions from the near-Earth plasma sheet, *J. Geophys. Res.*, *101*, 17,409–17,418.

Donovan, E., et al. (2008), Simultaneous THEMIS in situ and auroral observations of a small substorm, *Geophys. Res. Lett.*, *35*, L17S18, doi:10.1029/2008GL033794.

Dubyagin, S. V., V. A. Sergeev, C. W. Carlson, S. R. Marple, T. I. Pulkkinen, and A. G. Yahnin (2003), Evidence of near-Earth breakup location, *Geophys. Res. Lett.*, *30*(6), 1282, doi:10.1029/2002GL016569.

Dubyagin, S., V. Sergeev, S. Apatenkov, V. Angelopoulos, R. Nakamura, J. McFadden, D. Larson, and J. Bonnell (2010), Pressure and entropy changes in the flow-braking region during magnetic field dipolarization, *J. Geophys. Res.*, *115*, A10225, doi:10.1029/2010JA015625.

Evans, D. S., and M. S. Greer (2000), Polar Orbiting Environmental Satellite Space Environment Monitor 2: Instrument description and archive data documentation, *NOAA Tech. Memo., OAR SEC-93*, NOAA, Boulder, Colo.

Ganushkina, N. Y., T. I. Pulkkinen, M. V. Kubyshkina, V. A. Sergeev, E. A. Lvova, T. A. Yahnina, A. G. Yahnin, and T. Fritz (2005), Proton isotropy boundaries as measured on mid- and low-altitude satellites, *Ann.Geophys.*, *23*, 1839–1847.

Imhof, W. L., J. B. Reagan, and E. E. Gaines (1979), Studies of the sharply defined L dependent energy threshold for isotropy at the midnight trapping boundary, *J. Geophys. Res.*, *84*, 6371–6384.

Jussila, J. R. T., A. T. Aikio, S. Shalimov, and S. R. Marple (2004), Cosmic radio noise absorption events associated with equatorward drifting arcs during a substorm growth phase, *Ann. Geophys.*, *22*, 1675–1686.

Kirkwood, S., and L. Eliasson (1990), Energetic particle precipitation in the substorm growth phase measured by EISCAT and Viking, *J. Geophys. Res.*, *95*, 6025–6034.

Kubyshkina, M., V. Sergeev, N. Tsyganenko, V. Angelopoulos, A. Runov, E.Donovan, H. Singer, U. Auster, and W. Baumjohann (2011), Time-dependent magnetospheric configuration and breakup mapping during a substorm, *J. Geophys. Res.*, *116*, A00I27, doi:10.1029/2010JA015882.

Li, S.-S., V. Angelopoulos, A. Runov, X.-Z. Zhou, J. McFadden, D. Larson, J. Bonnell, and U. Auster (2011), On the force balance around dipolarization fronts within bursty bulk flows, *J. Geophys. Res.*, *116*, A00I35, doi:10.1029/2010JA015884.

Liang, J., E. F. Donovan, W. W. Liu, B. Jackel, M. Syrjäsuo, S. B. Mende, H. U. Frey, V. Angelopoulos, and M. Connors (2008), Intensification of preexisting auroral arc at substorm expansion phase onset: Wave-like disruption during the first tens of seconds, *Geophys. Res. Lett.*, *35*, L17S19, doi:10.1029/2008GL033666.

Lui, A., and J. Burrows (1978), On the location of auroral arcs near substorm onsets, *J. Geophys. Res.*, *83*, 3342–3348.

Lyons, L. R., I. O. Voronkov, E. F. Donovan, and E. Zesta (2002), Relation of substorm breakup arc to other growth-phase auroral arcs, *J. Geophys. Res.*, *107*(A11), 1390, doi:10.1029/2002JA009317.

Mende, S. B., et al. (2008), The THEMIS array of ground-based observatories for the study of auroral substorms, *Space Sci. Rev.*, *141*, 357–387.

Nakamura, R., A. Retinò, W. Baumjohann, M. Volwerk, N. Erkaev, B. Klecker, E. A. Lucek, I. Dandouras, M. André, and Y. Khotyaintsev

(2009), Evolution of dipolarization in the near-Earth current sheet induced by Earthward rapid flux transport, *Ann. Geophys.*, *27*, 1743–1754.

Newell, P. T., V. A. Sergeev, G. R. Bikkuzina, and S. Wing (1998), Characterizing the state of the magnetosphere: Testing the ion precipitation maxima latitude (b2i) and the ion isotropy boundary, *J. Geophys. Res.*, *103*, 4739–4745.

Nishimura, Y., L. Lyons, S. Zou, V. Angelopoulos, and S. Mende (2010a), Substorm triggering by new plasma intrusion: THEMIS all-sky imager observations, *J. Geophys. Res.*, *115*, A07222, doi:10.1029/2009JA015166.

Nishimura, Y., et al. (2010b), Preonset time sequence of auroral substorms: Coordinated observations by all-sky imagers, satellites, and radars, *J. Geophys. Res.*, *115*, A00I08, doi:10.1029/2010JA015832.

Paschmann, G., S. Haaland, and R. Treumann (Eds.) (2003), *Auroral Plasma Physics*, *Space Sci. Ser. ISSI*, vol. 15, Kluwer Acad., Dordrecht, Netherlands.

Pytte, T., H. Trefall, G. Kremser, L. Jalonen, and W. Riedler (1976), On the morphology of energetic (>30 keV) electron precipitation during the growth phase of magnetospheric substorms, *J. Atmos. Terr. Phys.*, *38*, 739–755.

Raeder, J., P. Zhu, Y. Ge, and G. Siscoe (2010), Open Geospace General Circulation Model simulation of a substorm: Axial tail instability and ballooning mode preceding substorm onset, *J. Geophys. Res.*, *115*, A00I16, doi:10.1029/2010JA015876.

Saito, M. H., L.-N. Hau, C.-C. Hung, Y.-T. Lai, and Y.-C. Chou (2010), Spatial profile of magnetic field in the near-Earth plasma sheet prior to dipolarization by THEMIS: Feature of minimum B, *Geophys. Res. Lett.*, *37*, L08106, doi:10.1029/2010GL042813.

Samson, J. C., L. R. Lyons, P. T. Newell, F. Creutzberg, and B. Xu (1992), Proton aurora and substorm intensifications, *Geophys. Res. Lett.*, *19*, 2167–2170, doi:10.1029/92GL02184.

Sergeev, V. A., and N. A. Tsyganenko (1982), Energetic particle losses and trapping boundaries as deduced from calculations with a realistic magnetic field model, *Planet. Space Sci.*, *30*, 999–1006.

Sergeev, V. A., E. M. Sazhina, N. A. Tsyganenko, J. A. Lundblad, and F. Soraas (1983a), Pitch-angle scattering of energetic protons in the magnetotail current sheet as the dominant source of their isotropic precipitation into the nightside ionosphere, *Planet. Space Sci.*, *31*, 1147–1155.

Sergeev, V. A., A. G. Yahnin, and R. J. Pellinen (1983b), Relative arrangement and magnetospheric sources of zones of energetic electron precipitation, diffuse and discrete auroras during the growth phase of a substorm, *Geomagn. Aeron., Engl. Transl.*, *23*, 972–978.

Sergeev, V. A., P. Tanskanen, K. Mursula, A. Korth, and R. C. Elphic (1990), Current sheet thickness in the Near-Earth plasma sheet during substorm growth phase, *J. Geophys. Res.*, *95*, 3819–3828.

Sergeev, V. A., M. Malkov, and K. Mursula (1993), Testing the isotropic boundary algorithm method to evaluate the magnetic field configuration in the tail, *J. Geophys. Res.*, *98*, 7609–7620.

Shevchenko, I. G., V. Sergeev, M. Kubyshkina, V. Angelopoulos, K. H. Glassmeier, and H. J. Singer (2010), Estimation of magnetosphere-ionosphere mapping accuracy using isotropy boundary and THEMIS observations, *J. Geophys. Res.*, *115*, A11206, doi:10.1029/2010JA015354.

West, H., Jr., R. Buck, and M. Kivelson (1978), On the Configuration of the magnetotail near midnight during quiet and weakly disturbed periods: Magnetic field modeling, *J. Geophys. Res.*, *83*, 3819–3829.

Xing, X., L. Lyons, Y. Nishimura, V. Angelopoulos, D. Larson, C. Carlson, J. Bonnell, and U. Auster (2010), Substorm onset by new plasma intrusion: THEMIS spacecraft observations, *J. Geophys. Res.*, *115*, A10246, doi:10.1029/2010JA015528.

Yago, K., K. Shiokawa, K. Hayashi, and K. Yumoto (2005), Auroral particles associated with a substorm brightening arc, *Geophys. Res. Lett.*, *32*, L06104, doi:10.1029/2004GL021894.

Yahnin, A. G., V. A. Sergeev, B. B. Gvozdevsky, and S. Vennerstrøm (1997), Magnetospheric source region of discrete auroras inferred from their relationship with isotropy boundaries of energetic particles, *Ann. Geophys.*, *15*, 943–958.

Zhou, X.-Z., V. Angelopoulos, V. A. Sergeev, and A. Runov (2011), On the nature of precursor flows upstream of advancing dipolarization fronts, *J. Geophys. Res.*, *116*, A03222, doi:10.1029/2010JA016165.

Zou, S., et al. (2010), Identification of substorm onset location and preonset sequence using Reimei, THEMIS GBO, PFISR, and Geotail, *J. Geophys. Res.*, *115*, A12309, doi:10.1029/2010JA015520.

V. Angelopoulos, Institute of Geophysics and Planetary Physics, University of California, Los Angeles, CA 90095, USA.

M. Kubyshkina and V. Sergeev, Institute of Physics, St. Petersburg State University, St. Petersburg, 198504, Russia. (victor@geo.phys.spbu.ru)

R. Nakamura, Space Research Institute, Austrian Academy of Sciences, Schmiedlstr. 6, A-8042 Graz, Austria.

Y. Nishimura, Department of Atmospheric and Oceanic Sciences, University of California, 405 Hilgard Ave., Los Angeles, CA 90095-1565, USA.

H. Singer, NOAA, 325 Broadway, Boulder, CO 80303, USA.